Ahsan Noor Khan

Multi-antenna systems for wireless capsule endoscopy

School of Electrical Engineering

Thesis submitted for examination for the degree of Master of Science in Technology.

Espoo 16.9.2016

Thesis supervisor:

Prof. Katsuyuki Haneda

Thesis instructor:

M.Sc. Miah Md Suzan

Aalto University
School of Electrical
Engineering

AALTO UNIVERSITY
SCHOOL OF ELECTRICAL ENGINEERING

ABSTRACT OF THE
MASTER'S THESIS

Author: Ahsan Noor Khan

Title: Multi-antenna systems for wireless capsule endoscopy

Date: 16.9.2016 Language: English Number of pages:10+44

Department of Radio Science and Engineering

Professorship: Radio Science Code: S-26

Supervisor: Prof. Katsuyuki Haneda

Instructor: M.Sc. Miah Md Suzan

With the advent of new medical diagnostic techniques, the wireless capsule endoscopy has been emerged as more convenient than traditional endoscopy for the digestive tract monitoring. The typical use of wireless capsule endoscopy is to diagnose intricate areas of the small intestine. However, the current wireless capsule endoscopy systems suffer from low data rate which cannot meet the requirement for transmitting high resolution images. The poor quality of received images can bring ambiguities during the diagnosis.
In this master thesis, the MIMO antennas employing polarization diversity is proposed for a wireless capsule endoscopy system at 433 MHz ISM band. The polarization diversity between in-body capsule and on-body receiver is considered to be main responsible for increasing the data rate. Two conformal dual polarized loop antennas are designed for the in-body capsule transmitter, while two planar dual polarized printed monopole antennas are designed for the on-body receiver. The on-body receiving antennas are designed using the flat and flexible substrates to study their impacts on the size, bandwidth and efficiency.

The simulated refection coefficients of proposed in-body MIMO antennas are less than -10 dB over the required bandwidth (400-500 MHz). The mutual coupling between them is found to be less than -20 dB over a wide range of frequencies. The on-body MIMO antennas are measured on the liquid phantom to validate the simulated results. The simulated and measured results showed good agreement of matching in terms of reflection coefficients and mutual coupling. Moreover, the size of on-body antennas found to be compact by using the high permittivity substrate. The on-body MIMO antennas are also measured on the human body. It is observed that the lossy properties of skin significantly reduce the mutual coupling between the MIMO antennas.

Keywords: MIMO, conformal loop antennas, body phantom, printed monopole antennas, dielectric loading effect, mutual coupling, liquid phantom

Acknowledgments

This master's thesis is based on research work conducted at the Department of Radio Science and Engineering (RAD) Aalto University, School of Electrical Engineering.

First and foremost, I would like to express my deepest gratitude to my supervisor Prof. Katsuyuki Haneda who has supported throughout my thesis work with his patience, motivation and immense knowledge. I am highly obliged to be a part of his research group which helped me in exploiting my potential. His suggestions and feedbacks have supported me to achieve desired results in the most efficient way.

I am heartily thankful to my instructor Miah Md Suzan whose encouragement, supervision and support from the preliminary to the concluding level enabled me to develop good understanding of the subject. I would like to thank Mikko Heino for his help and guidance in the antenna fabrication process.

I would like to thank Dr. Jari Holopainen and Dr. Clemens Icheln for their valuable suggestions and comments regarding the antenna design and simulation.

Lastly, I am indebted to my parents Mr & Mr.s Dr.Noor-ul-islam khan and family members for their support and prayers during my studies. Special thanks to my elder brother Hasan Noor Khan for his motivation and encouragement that helped me to remain focus on my studies.

Above all, I would like to thank God Almighty, for his blessings and support during my studies.

Ahsan Noor Khan

Otaniemi, 16.9.2016

Contents

Abbreviations and Acronyms

BAN	Body area network
EM	Electromagnetic
EGD	Esophagogastroduodenoscopy
ISM	Industrial Scientific Medical
MICS	Medical Implant Communication Service
MIMO	Multiple-input-multiple-output
UWB	Ultra-wideband
UV	Ultraviolet
WCE	Wireless capsule endoscopy

Symbols

ϵ	Permittivity
σ	Conductivity
$\tan\delta$	Loss tangent

List of Figures and Tables

List of Figures

List of Tables

1 Introduction

The importance of healthcare technologies in improving the quality of life is broadly well recognized. For several decades, imaging techniques, such as x-ray, ultrasound and computerized tomography have been mostly used to diagnose diseases inside the human body. To acquire reliable diagnosis in the medical field, microwaves and radio waves have received much more attention, thus leading to the use of implantable medical devices [1]. In the earlier use of implantable medical devices, wireless technology was not very common. However, the latest research in understanding the interaction between electromagnetic (EM) waves and human body has facilitated health monitoring with wireless implantable devices.

One of the important possible applications of wireless implantable devices is wireless capsule endoscopy (WCE) which is used to record images of the digestive tract for diagnosis [2]. A typical advantage of the capsule endoscopy is to examine convoluted areas of the small intestine that cannot be seen by other two types of endoscopy, such as colonoscopy and esophagogastroduodenoscopy (EGD). A colonoscopy is a lower endoscopy technique and it is inserted through the rectum of the digestive tract. It can record images of the colon and distal portion of the small intestine, while the EGD is used to examine esophagus, stomach and the first part of the small intestine. These two types of endoscopy are not able to visualize majority of the small intestines middle portion. In addition, these endoscopy techniques are still painful and time consuming. On the other hand, capsule endoscopy is non-invasive, painless and requires no sedation [3]. It can comfortably diagnose bleeding, iron deficiency, abdominal pain and tumors in the small intestine.

The procedure of capsule endoscopy entails swallowing a wireless capsule about a size of a multi-vitamin that has a tiny camera attached to it. The capsule moves through the digestive tract and takes images. The captured images are transmitted to the on-body receiving unit. Physicians can interpret the images for diagnosis in the real time or offline. A typical WCE system is shown in Fig. 1.

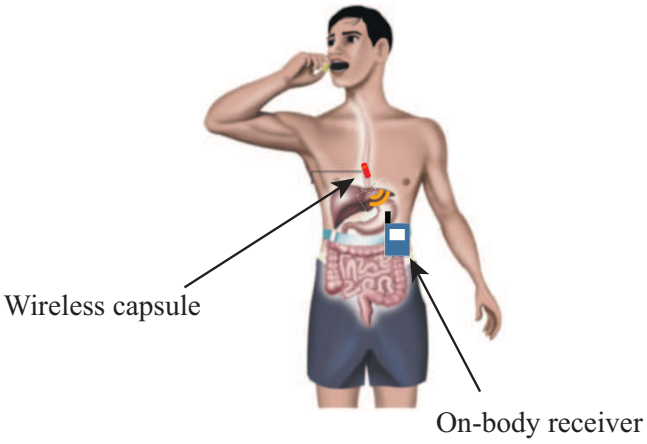

Fig. 1: Wireless capsule endoscopy system.

A wireless capsule consists of several components, such as illuminating light emitting diode (LED), lens, camera, batteries, ASIC (application specific integrated circuit) transmitter and an antenna as shown in Fig. 2. Among other components in the wireless capsule, antenna is an important element for wireless communication with the on-body receiver. This particular master thesis focuses on antenna solutions for a WCE system.

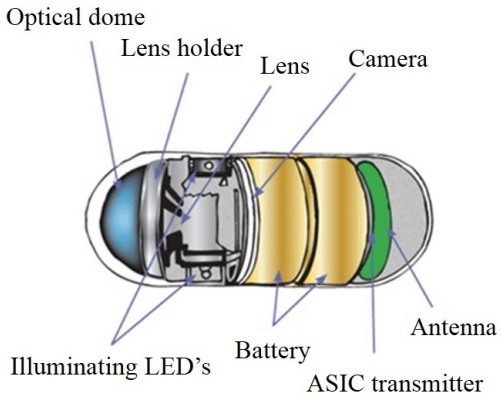

Fig. 2: Wireless capsule structure.

In a wireless capsule endoscopy (WCE) system, the quality of received images plays an important role for the reliable diagnosis by physicians. A minimum 3.5 Mb/s data rate is required for sufficient quality of images [4], whereas 110 Mb/s data rate is required to receive video [5]. Recently, considerable research has been devoted to improve the data rate for receiving high resolution images. In [6], an approach based on image compression technique was used to increase the frame rate of the received images, while a low complexity video encoding method was used in [7]. The high power consumption and intensive computations in the capsule are the main challenges in implementing image compression and encoding schemes. Another approach to improve the data rate of a WCE system is the use of ultra-wideband (UWB) technology as presented in [8–10]. However, the absorption of EM waves in the body tissues are more at higher frequencies which increases the propagation loss between the capsule transmitter and on-body receiver. For instance, propagation losses in the human body increases exponentially for frequencies above 1.5 GHz [11]. In order to avoid high propagation losses in the body tissues, most of the commercially available WCE systems operate at low frequency bands, such as industrial scientific and medical (ISM, 433-434.8 MHz) and medical implant communication service (MICS, 402-405 MHz) [12, 13]. The channel bandwidth in these bands is not sufficient to support high data rate communication through the body.

The multiple-input-multiple-output (MIMO) technique has been one of the most promising method for increasing wireless performance in terms of data throughput and reliability. The MIMO antennas employing polarization diversity scheme in a wireless system can increase the data rate without additional bandwidth. In

[14] and [15], a transmit polarization diversity scheme was used in the implant to improve the data rate at ultra-wideband (UWB) frequencies (3.4-4.8 GHz). Two orthogonal planar elliptical loop antennas were used in the implant to communicate with multiple on-body receiving antennas. However, the propagation losses in the body tissues are more at ultra-wideband frequencies as compared to MICS and ISM bands.

This master thesis presents the design and analysis of dual polarized MIMO antennas for in-body capsule and on-body receiver to increase the data rate of a WCE system. The unlicensed 433 MHz ISM band is selected to reduce the propagation losses through the body tissues. Moreover, according to the best of author knowledge, no experimental validation is reported in the literature for a multi-antennas WCE system at 433 MHz ISM band.

The objective of this thesis is to design dual polarized MIMO antennas for the in-body capsule transmitter and on-body receiver at 433 MHz ISM band. For this purpose, two orthogonal conformal loop antennas have been designed for the capsule transmitter, whereas two orthogonal printed monopole antennas have been designed, simulated and measured for the on-body receiver. As the distance between the capsule transmitter and on-body receiver is small, polarization diversity scheme will be mainly responsible for increasing the data rate. However, the analysis of potential increase in the data rate is considered for future work.

The rest of thesis is organized as follows: Chapter 2 describes the human body characteristics and human equivalent tissue models. The in-body capsule antenna design and simulation results are presented in chapter 3. Chapter 4 reports the design and simulations results for on-body receiving antennas. Measurement results of the on-body antennas are described in chapter 5. Chapter 6 presents the conclusions and future areas of research in the WCE systems.

2 Human Body Characteristics and Tissue Models

Recent developments in the communication technologies have enabled the use of wireless communication for improving health care. Thus, the body area networks (BANs) are becoming an emerging technology for their applications in the medical field. The BANs are wireless networks in which sensors are placed over the human body. There are two main categories of BANs, such as wearable and implantable. A wearable BAN operates on the surface of the human body, while an implantable BAN operates inside [16]. They have distinctive features and requirements as compared to the traditional wireless networks. For instance, they need to operate with specified power levels so that the exposure of electromagnetic waves to humnan body can be reduce [17]. In Fig. 3, a typical wearable BAN application in health care is shown in which many sensors are placed over the body to communicate with an on-body base station. The base station collects information from the sensors and process it for monitoring various physiological data, for example blood temperature, body motion and so on.

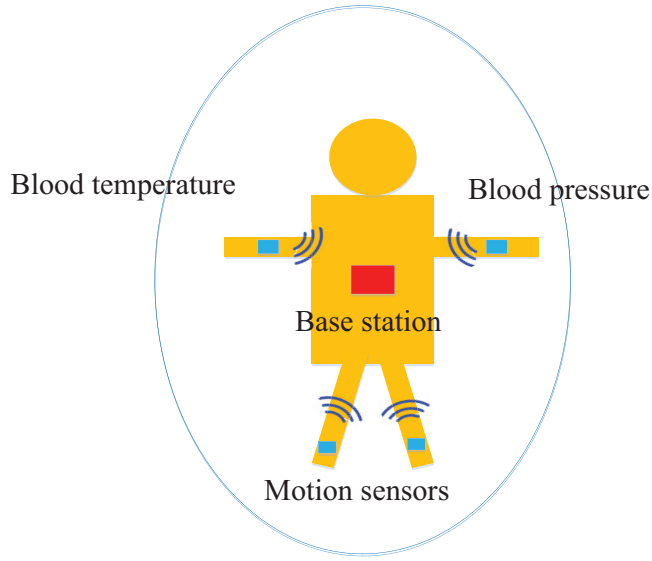

Fig. 3: Wearable BAN application in health care [18].

For diagnosing diseases inside the human body, the implantable BANs are mostly used. They exhibit distinguished features as compared to wearable BANs, such as compact size, battery power limitations and signal transmission through the lossy tissues. The wireless capsule endoscopy is a typical example of an implantable BAN where an ingestible wireless capsule is used to record images of the digestive tract [2]- [15].

2.1 Electrical properties of the body tissues

The human body is an inhomogeneous, lossy and dispersive medium. It consists of several tissues. The tissues vary in their composition and electrical properties, such as permittivity, conductivity and loss tangent [19]. These electrical properties are frequency dependent and affect the performance of an antenna in their close proximity. Fig. 4 shows the permittivity and conductivity of skin, fat, muscle and colon tissue as a function of frequency [20]. Fat is a low water content tissue with significantly different dielectric properties than skin, muscle and colon tissue. The conductivity of tissues increases with frequency, while permittivity decreases.

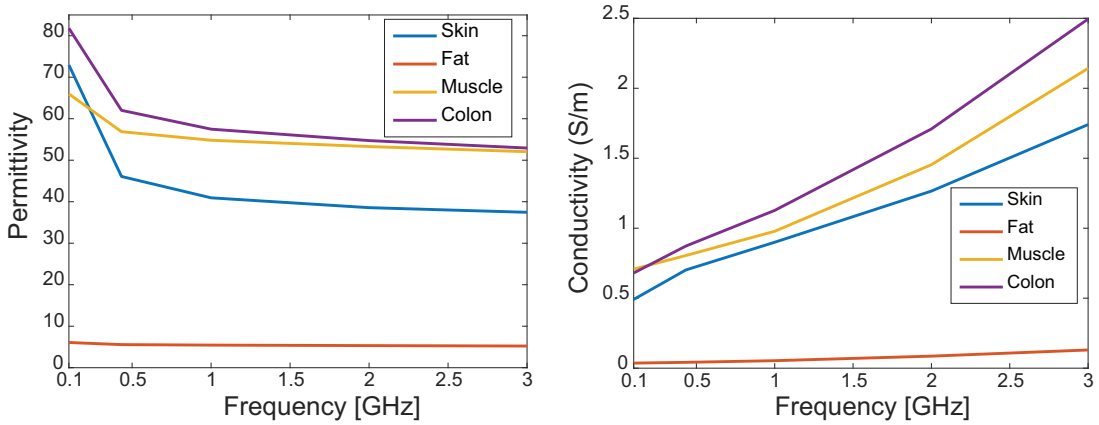

(a) (b)

Fig. 4: Electrical properties of the skin, fat, muscle and colon tissues: (a) permittivity; (b) conductivity.

2.2 Impacts of the body tissues on an antenna performance

The electrical properties of body tissues affect the characteristics of an antenna, such as electrical length, radiation efficiency and gain. The electrical length of an implantable and on-body antenna increases due to high permittivity of the surrounding body tissues. Therefore, a lower resonant frequency is obtained as compared to the free space scenario for the given fixed dimensions of an antenna . This phenomena is called as dielectric loading effect and the amount of detuning depends on the antenna distance from the body tissues. For example, Fig. 5 shows the simulated reflection coefficient of an implantable antenna when it is placed in the free space and colon tissue. It is observed that the high permittivity colon tissue ($\epsilon = 62.019$) detunes the antenna towards lower frequencies by increasing its electrical length as compared to the free space ($\epsilon = 1$).

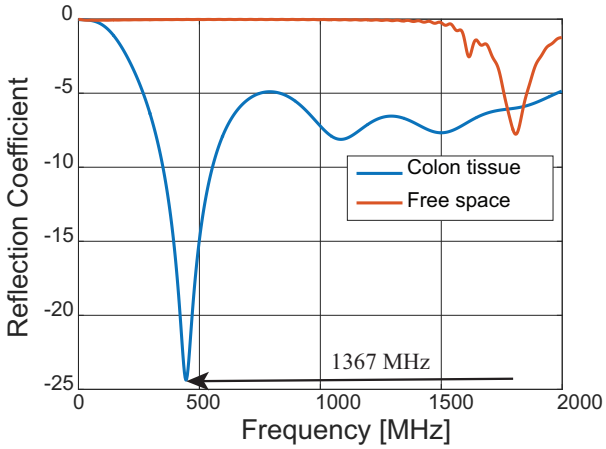

Fig. 5: Dielectric loading effect on an implantable antenna due to the high permittivity of colon tissue.

The power radiated from an antenna defines it efficiency. For any antenna in free space, the radiated power mainly depends on the far field components as the near field is mainly reactive [21]. However, the near fields of an implantable and on-body antenna strongly couples in the surrounding tissues. Thus, tissues absorb most of the radiated power and decrease the efficiency of an implantable antenna.

2.3 Human equivalent tissue models

The dielectric properties of body tissues have significant effect on the performance of an implantable and on-body antenna. Thus, it becomes essential to study the antenna performance inside the inhomogeneous lossy medium. For numerical simulations, the implantable antennas are mostly studied inside the human body that simulate biological tissues. The computational cost heavily depends on the complexity of the tissues models. There are three main types of tissue models which are being used for numerical simulations, such as canonical, anatomical and full body model.

2.3.1 Canonical tissue model

For speeding up the simulations with appropriate dielectric properties, canonical geometries, such as rectangular cuboid box [22–24], cylindrical [25,26] and spherical tissue models [27] are mostly used in literature. The shape of canonical tissue models can be selected according to the application of interest. These tissue models can be single layered or multilayered. A single layered tissue model is shown in Fig. 6(a). It takes less time to compute but ignores reflections in the multiple layers of the body tissues. In contrast, a multilayered canonical tissue model provides accurate estimation of reflections and absorptions in different body tissues [28]. Fig. 6(b) shows an implantable antenna inside a four layered canonical tissue model which consists of skin, fat, muscle and colon tissues.

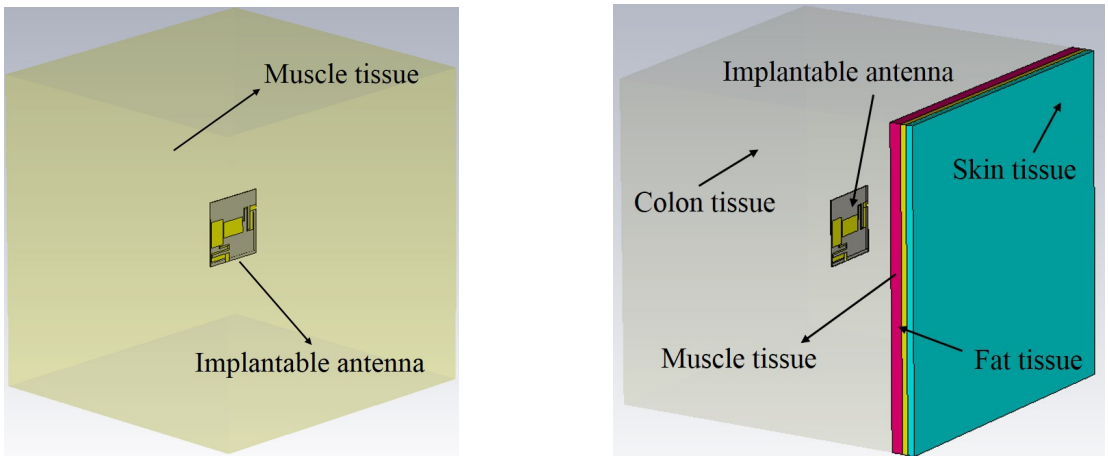

(a) (b)

Fig. 6: Canonical tissue models: (a) single layered; (b) multilayered.

2.3.2 Anatomical tissue model

The anatomical tissue model provides more realistic results as compared to the canonical tissue model. It improves the accuracy of the design but requires more computational time. Fig. 7(a) shows anatomically defined chest model from ANSYS human body model.

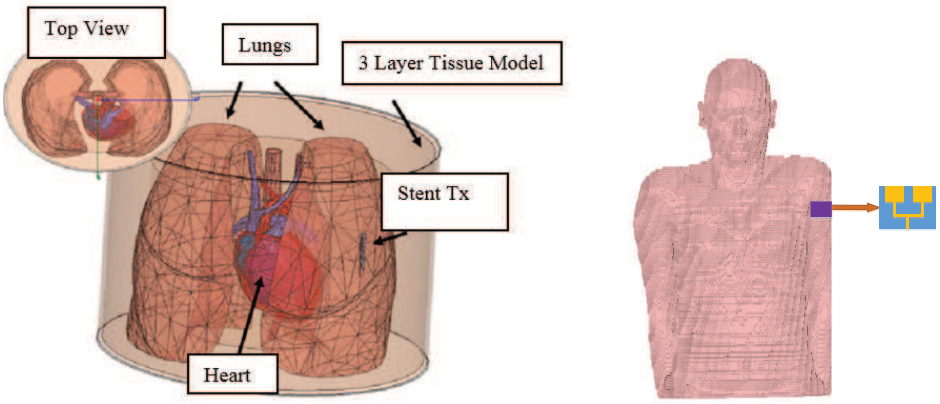

(a) (b)

Fig. 7: Tissue model: (a) anatomically defined chest model from ANSYS [29]; (b) Laura voxel full body model from CST [30].

2.3.3 Full body models

These are the most comprehensive body models which provide the highest level of accuracy in the numerical study. However, they require longer simulation time. In [31], the complete Japanese males and female computational body models were

designed for the electromagnetic dosimetry. A Laura voxel body model for characterizing the performance of an on-body wearable antenna is shown in Fig. 7(b).

2.4 Human equivalent phantom models

The experimental investigations are required to validate the results obtained from numerical simulations of an implantable or on-body antenna. Due to safety guides by the Federal Communications Commission, a human body cannot be used for the experimental investigations of an implantable antenna. Therefore, tissue equivalent phantoms and animal tissues are mostly used to characterize the performance of an implantable antenna.

2.4.1 Tissue equivalent phantom

The testing of an implantable antenna is convenient to perform inside the tissue equivalent phantom. A tissue phantom is usually a container filled with liquid or gel material that behaves electrically similar as an implant tissue. There are several recipes available to formulate the tissue equivalent liquid or gel. For example in [24], an implantable antenna is tested in a skin mimicking gel which is composed of deionized water, sugar, salt and agarose. In [32], a liquid with the muscle tissue properties is formulated by mixing sugar, salt and water. Fig. 8 shows single layer liquid phantom which is used to test an implantable capsule antenna.

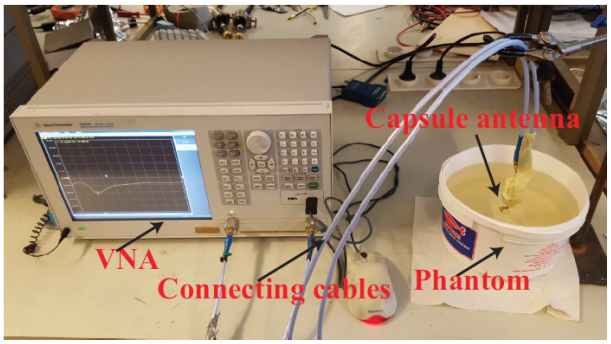

Fig. 8: Antenna testing inside a muscle mimicking liquid phantom [32].

2.4.2 Testing with animal tissue

The use of animal tissues provide realistic approach in the design verification of an implantable antenna. The implantable antenna can be tested either by embedding in the tissue samples from a donor animal i.e. *ex-vivo* studies or by implanting the antenna inside live animal by using surgical methods i.e. *in-vivo* studies. Fig. 9(a) shows the implantation of an antenna inside the rat skin for performing *ex-vivo* studies. To further assess the performance on an implantable antenna in real scenario, *in-vivo* studies are performed as shown in Fig. 9(b).

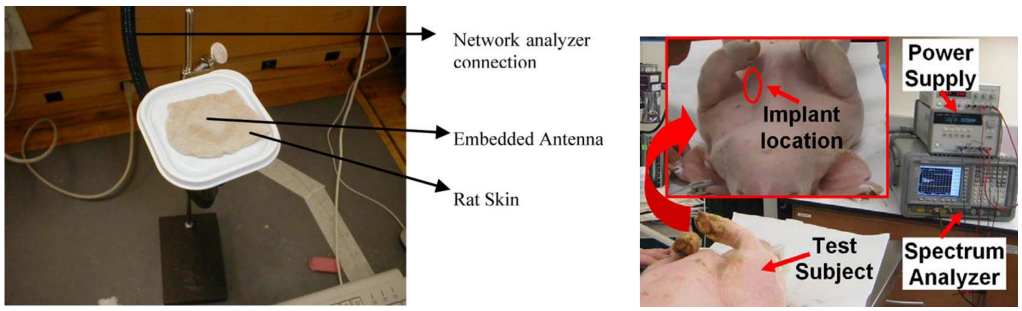

(a) (b)

Fig. 9: Implantable antenna testing with animal tissue: (a) antenna inside the rat skin [33]; (b) antenna inside the porcine test subject [29].

3 Design and Analysis of Dual Polarized MIMO Antennas for the in-body Capsule Transmitter

In a WCE system, the transmitting antenna of a capsule module plays vital role for establishing robust communication links with an on-body receiver. This chapter describes the design and simulation results of the dual polarized MIMO antennas for an in-body capsule transmitter. Two orthogonal conformal loop antennas are proposed at 433 MHz. One loop antenna is conformed on the inner surface of the capsule shell, while a second loop antenna utilizes the outer surface. The performance of both loop antennas is evaluated inside a body phantom with the properties of colon tissue which is an integral part of the digestive tract. The CST microwave studio is used for the design and simulation of dual polarized MIMO antennas.

This chapter is organized as follows: Section 3.1 presents the design challenges for an in-body capsule transmitting antenna. The different types of capsule antenna structures and the design of MIMO antennas are described in Section 3.2. The body phantom properties are presented in Section 3.3. Simulation results of the MIMO antennas are described in Section 3.4. The impacts of capsule orientations on the performance of MIMO antennas are presented in Section 3.5. The chapter summary is described in Section 3.6.

3.1 Antenna for an in-body capsule transmitter

3.1.1 Design challenges and requirements

There are certain challenges and requirements to design an antenna for the in-body capsule transmitter. For instance, an antenna should have compact size due to limited available space in the capsule module. The diameter of capsule module is 11 mm and its shell is made of 0.5 mm thick Ultem material ($\epsilon_r = 3.5$ and $\tan\delta = 0.00027$) as shown in Fig. 10. However, the antenna size becomes large at 433 MHz ($\lambda_{air} =$ 692 mm) and miniaturization techniques are required for its placement.

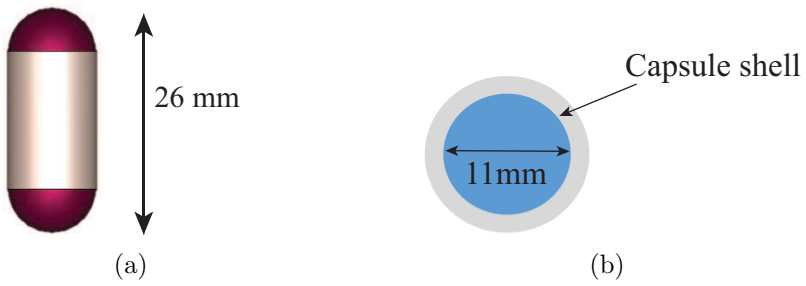

Fig. 10: Capsule module: (a) side view; (b) cross section view.

Once the capsule is swallowed by the patient, it travels through the entire digestive tract which is composed of several tissues with different dielectric properties. Thus, it experiences a diverse propagation environment during the travel period. Therefore, ultra-wide operational bandwidth is required for an antenna to exhibit robustness against the detuning. In addition, an antenna should have omnidirectional pattern in order to maintain the continuous communication with an on-body receiver irrespective of the capsule orientation.

3.2 Antenna structures for an in-body capsule transmitter

There are two promising antenna types which have been reported in the literature, such as embedded [34] and conformal [35–37] antenna structures. Fig. 11(a) and Fig. 11(b) shows the embedded and conformal antenna structures respectively for the in-body capsule transmitter. The embedded antennas are placed inside the capsule module, while conformal antenna structures are designed on the surface of a capsule module. The conformal antenna only occupies the surface of a capsule module and leaves the interior portion for other electronic components. Thus, the size of a capsule module can be reduced as compared to an embedded antenna structure.

(a) (b)

Fig. 11: Antenna types for a capsule transmitter: (a) embedded antenna inside a capsule module; (b) conformal antenna around the outer surface of a capsule module.

The antenna of an in-body capsule transmitter should be less sensitive to the lossy properties properties of body tissues. For this reason, magnetic loop antennas are mostly preferred for the capsule as they are less sensitive to influence by the body tissues than other electrical antenna types, such as dipoles and monopoles [32]. In this section of the chapter, the MIMO antennas for an in-body capsule transmitter are proposed. One conformal loop antenna is designed on the outer surface of capsule shell, while second conformal loop antenna utilizes the inner shell.

3.2.1 Outer shell loop antenna

Fig. 12(a) shows the geometry of outer shell loop antenna which is patterned on a 0.55 mm thick flexible substrate called as Polyimide ($\epsilon = 3.5$ and $\tan\delta = 0.0003$). The flexible nature of Polyimide material helps in conforming antenna on the outer surface of capsule shell as shown in Fig. 12(b).

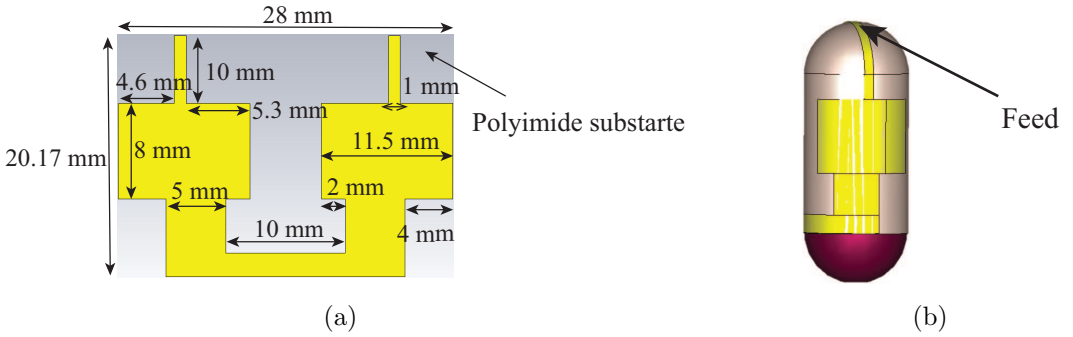

Fig. 12: Outer shell loop antenna structure: (a) before; (b) after conforming on the outer surface of a capsule shell.

3.2.2 Inner shell loop antenna

An antenna around the inner surface of capsule shell is 0.5 mm away from the body tissues. Therefore, the dielectric loading effect is lower as compared to an antenna on the outer surface of capsule shell. To miniaturize the antenna dimensions, meander lines are used as they increase the electrical length within compact dimensions. The configuration of inner shell loop antenna before and conforming on the inner surface of capsule shell is shown in Fig. 13. The antenna is designed on the same substrate material which is used for the outer shell loop antenna. Two feed lines of 7.5 mm length and 0.5 mm width are used to form the loop.

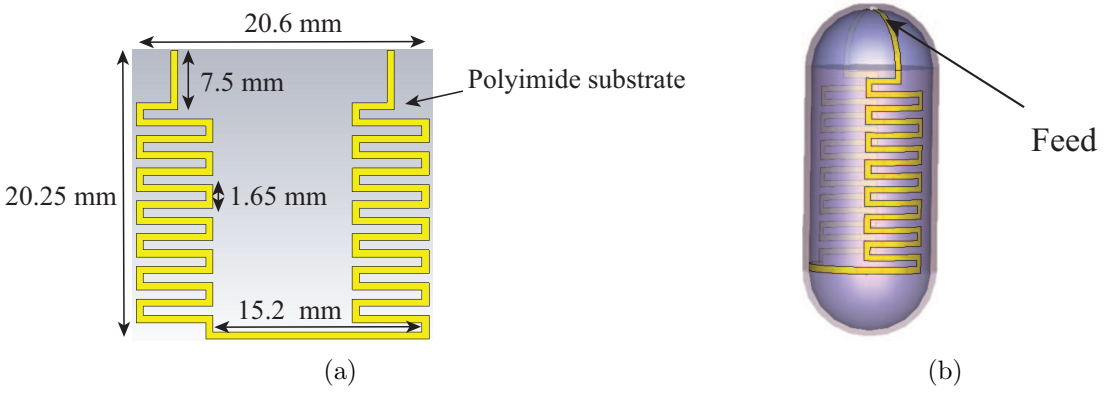

Fig. 13: Inner shell loop antenna structure: (a) before; (b) after conforming on the inner surface of capsule shell.

3.2.3 MIMO antennas for the in-body capsule transmitter

The designed inner and outer shell loop antennas are now conformed together around the capsule module as shown in Fig. 14(a). The antennas are placed orthogonal to each other in order to obtain dual polarization in the capsule transmitter. The feed

lines of both inner and outer shell loop antennas are shown in Fig. 14(b).

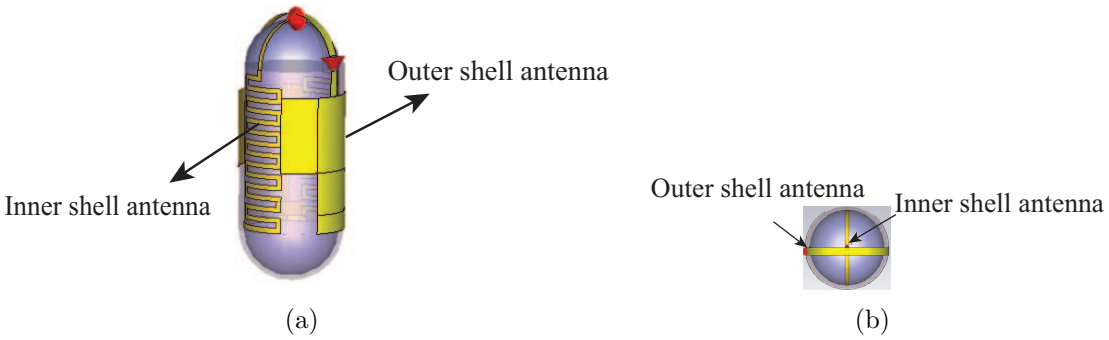

Fig. 14: MIMO antennas for the in-body capsule transmitter: (a) conformed around the capsule shell; (b) feeding structure for dual polarization.

3.3 Human equivalent tissue model for simulation

A rectangular single layered canonical tissue model with the colon tissue properties ($\epsilon = 62.019$ and $\tan\delta = 0.58719$ at 433 MHz) is used to simulate the MIMO antennas of the in-body capsule transmitter. The colon tissue equivalent tissue model is shown in Fig. 15. Moreover, the size and shape of the tissue model is similar to the body phantom which will be used for performing measurements. The body phantom is 0.5 mm thick plastic ($\epsilon = 1.9$ and $\tan\delta = 0.003$) rectangular box that contains the colon tissue equivalent liquid.

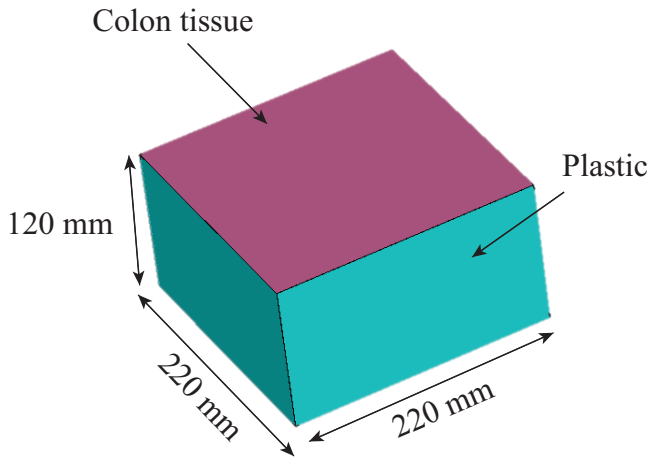

Fig. 15: Rectangular shaped single layer canonical tissue model with the colon tissue properties at 433 MHz.

3.4 Simulation results of MIMO antennas inside the body phantom

To study the performance of MIMO antennas in realistic environment, the capsule module is placed at the center of body phantom as shown in Fig. 16. Port 1 is assigned to the inner shell loop antenna, while port 2 is used for the outer shell loop antenna. The MIMO antennas are simulated for characterizing their performance in terms of reflection coefficient and mutual coupling.

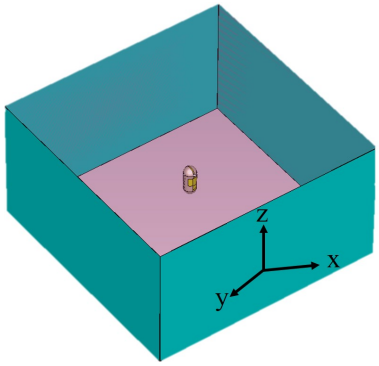

Fig. 16: Capsule module at the center of body phantom.

3.4.1 Reflection coefficients

The simulated reflection coefficients are shown in Fig. 17. The reflection coefficients of inner and outer shell loop antennas at 433 MHz are -21.66 dB and -33.02 dB respectively. The reflection coefficient of outer shell loop antenna is less than -10 dB over a wide bandwidth. In contrast, the inner shell loop antennas has shown narrow -10 dB bandwidth (336-540 MHz) due to meander lines inductance and compact dimensions.

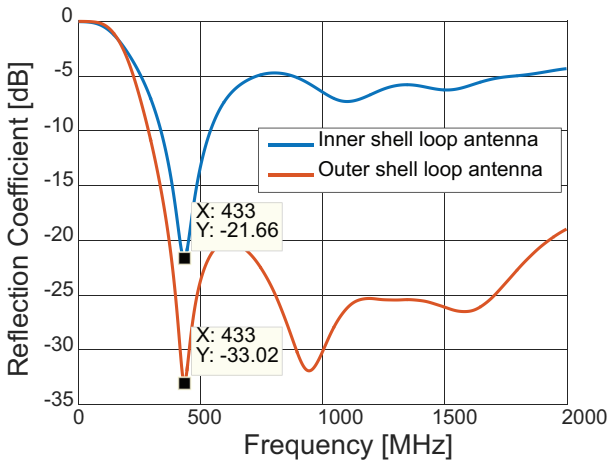

Fig. 17: Simulated reflection coefficients of the MIMO antennas.

3.4.2 Mutual coupling

The simulated mutual coupling ($|S_{21}| = |S_{12}|$) is less than -20 dB over a wide bandwidth as shown in Fig. 18. The low mutual coupling is due to 0.5 mm thick capsule shell which prevents the flow of electric current between the MIMO antennas.

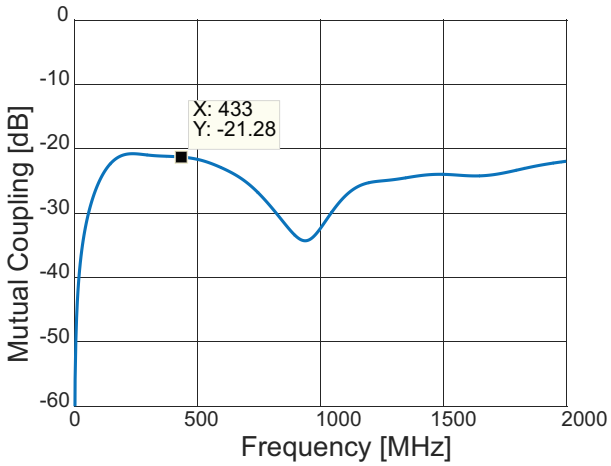

Fig. 18: Simulated mutual coupling between the MIMO antennas.

3.5 Analysis of MIMO antennas performance with different capsule orientations

The capsule swallowed by the patient undergoes random orientations while moving through the digestive tract. Therefore, it is important to study the impacts of capsule orientations on the performance of MIMO antennas. The MIMO antennas are simulated with three different orientations of the capsule as shown in Fig. 19.

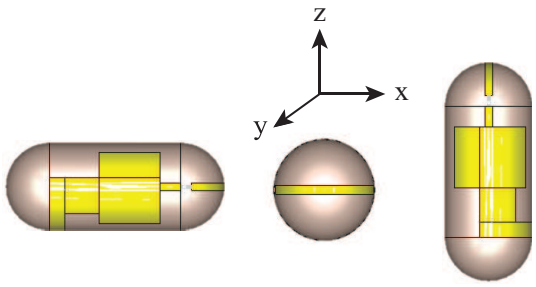

Fig. 19: Three different orientations of the capsule.

The simulated reflection coefficients are shown in Fig. 20. It is observed that the MIMO antennas have not detuned despite the capsule orientations. Thus, the capsule orientations have insignificant impact on the reflection coefficients of MIMO

antennas. Moreover, the reflection coefficients are less than -10 dB in the required bandwidth (400-500 MHz) irrespective to the capsule orientations.

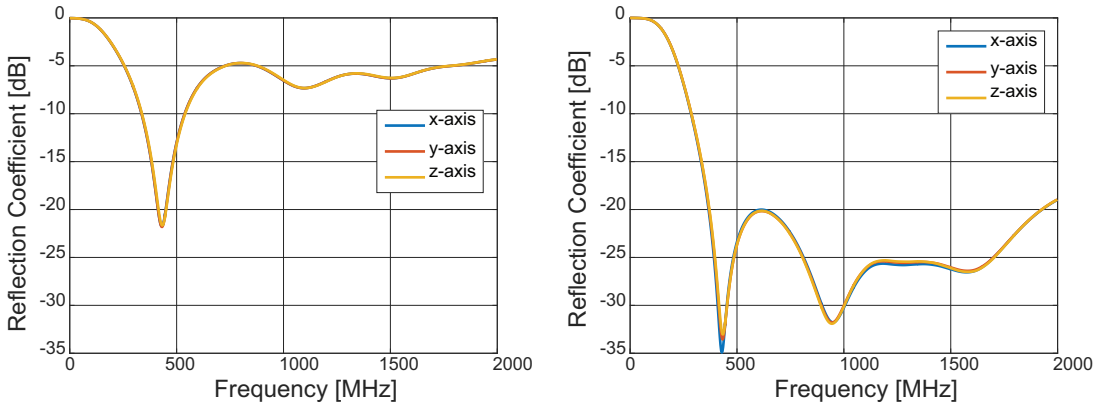

(a) (b)

Fig. 20: Simulated reflection coefficients for the capsule orientations: (a) inner shell loop antenna; (b) outer shell loop antenna.

The simulated mutual coupling ($|S_{21}|=|S_{12}|$) is illustrated in Fig. 21. It can be seen that the MIMO antennas have maintained good level of isolation over a wide range of frequencies. Thus, the design of MIMO antennas is robust against the capsule orientations.

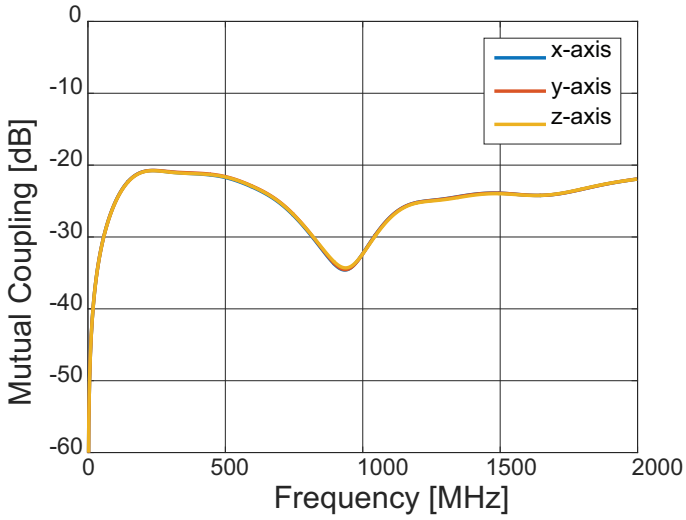

Fig. 21: Simulated mutual coupling between MIMO antennas for three capsule orientations.

3.6 Chapter summary

In this chapter, the design and analysis of dual polarized MIMO antennas were presented for the capsule transmitter in a WCE system. One conformal loop antenna was designed on the inner surface of capsule shell, while the second loop antenna utilized the outer surface. The antennas were conformed orthogonal to each other to obtain dual polarization in the capsule transmitter. The performance of MIMO antennas was characterized inside the rectangular shaped body phantom with colon tissue properties at 433 MHz. From the simulated results, it was found that the reflection coefficients of dual polarized MIMO antennas were less than -20 dB at 433 MHz. Moreover, the -10 dB bandwidth of inner shell loop antenna was narrow as compared to the outer shell loop antenna. The mutual coupling between MIMO antennas was also studied in this chapter. It was observed that the mutual coupling is less than -20 dB over a wide bandwidth. Lastly, the impact of capsule orientations on the performance of MIMO antennas was studied. It was found that the MIMO antennas showed robustness against the detuning and maintained good level of matching and isolation at 433 MHz.

4 Design and Analysis of Dual Polarized MIMO Antennas for the On-body Receiver

In the context of receiving high quality images, a WCE system requires an efficient on-body antenna. The on-body antenna should be flexible and compact in size in order to ensure the comfortability for patients. However, the dielectric loading effect of body tissues is lower for an on-body antenna as compared to an in-body antenna. Thus, the design of compact size and efficient on-body antenna is a challenging task at 433 MHz ISM band.

In this part of the thesis, the design and analysis of dual polarized MIMO antennas are presented for an on-body receiver of a WCE system. The performance of MIMO antennas are characterized using the flat and flexible substrates. The FR-4 and RT Duroid are used as flat substrates, while a 0.55 mm thick material is used as flexible substrate. The motivation of considering different substrates is to determine their impacts on the size, flexibility, bandwidth and efficiency of MIMO antennas. Moreover, meander lines are used in the antenna structures for their considerable miniaturization at 433 MHz. The body phantom with the colon tissue properties is used to characterize the performance of the designed antenna structures.

The chapter is organized as follows: Section 4.1 describes the design and analysis of on-body MIMO antennas using the FR-4 substrate. In Section 4.2, the MIMO antennas are simulated using the RT Duroid substrate. Moreover, separate ground planes are proposed to reduce the mutual coupling between MIMO antennas. In section 4.3, the MIMO antennas are designed and simulated using the flexible substrate. The chapter summary is presented in Section 4.4.

4.1 Design and analysis of on-body MIMO antennas using the FR-4 substrate

Printed monopole antennas are being used in various wireless systems due to their light weight and low cost of fabrication. They belong to the monopole antennas family and have a radiating element on the top side of substrate. The ground plane is designed on the bottom side of substrate and its dimensions affect the antenna resonant frequency. In this section, two orthogonal printed monopole antennas are designed on the commonly available 1.5 mm thick FR-4 substrate ($\epsilon = 4.3$ and $\tan\delta = 0.025$).

4.1.1 Geometry of the MIMO antennas structure

The geometry of proposed MIMO antennas structure is shown in Fig. 22. It consists of dual polarized printed monopole antennas on the FR-4 substrate with the size of 87 mm $\times$ 87 mm. Moreover, the meander lines and common ground plane are used to increase the electrical length of each printed monopole antenna for compact dimensions at 433 MHz.

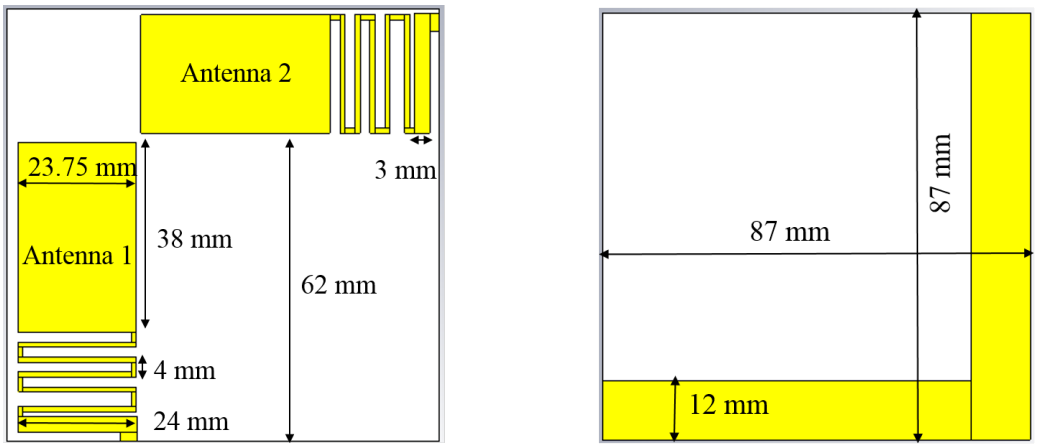

Fig. 22: Geometry of the MIMO antennas structure using the FR-4 substrate: (a) top view; (b) bottom view.

4.1.2 Simulation set-up and results

The designed MIMO antennas structure is placed on the body phantom as shown in Fig. 23. The simulated environment is designed with respect to the measurement set-up. For instance, the SMA connectors of printed monopole antennas will keep the antenna structure approximately 2 mm away from the body phantom. Therefore, the air gap is considered in the simulation environment to validate the measurement set-up. The antenna structure is simulated by assigning port 1 and port 2 to antenna 1 and antenna 2 respectively.

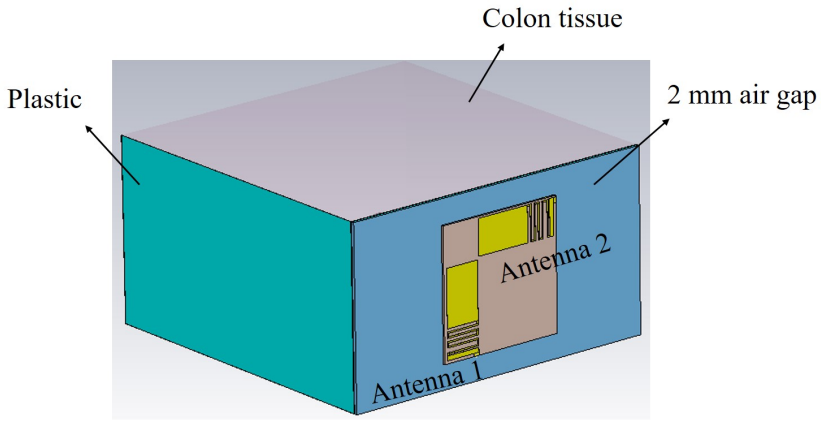

Fig. 23: MIMO antennas structure on the body phantom.

The simulated reflection coefficients of the MIMO antennas are shown in Fig. 24. It is observed that the MIMO antennas are well matched at 433 MHz. The simulated reflection coefficients of antenna 1 and antenna 2 at 433 MHz are -19.64 dB and -

21.44 dB respectively. Moreover, the -10 dB impedance bandwidth of both printed monopole antennas is 145 MHz (365-510 MHz).

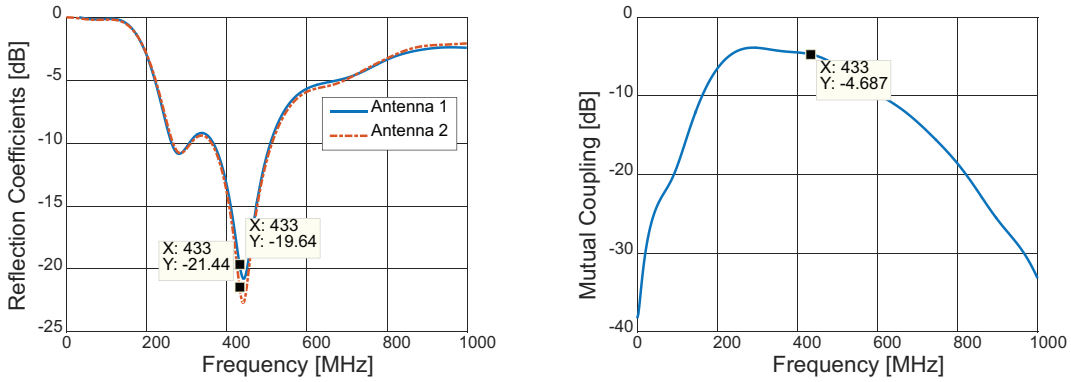

(a) (b)

Fig. 24: Simulated results of MIMO antennas using the FR-4 substrate: (a) reflection coefficients; (b) mutual coupling.

On the common ground plane, the electric current which is flowing between the antenna ports is mainly responsible for mutual coupling. The lossy properties of colon tissue absorb the flow of electric and decrease the mutual coupling. As the antenna structure moves towards the body phantom, the absorption of electric current on the common ground plane increases. However, in our simulation environment, the antenna structure is 2 mm away from the body phantom. Thus, the impact of colon tissue is less significant for reducing the mutual coupling. The simulated mutual coupling ($|S_{12}|$=$|S_{21}|$) between MIMO antennas is -4.687 dB at 433 MHz as shown in Fig. 24(b).

The simulated gain and total efficiency of MIMO antennas are shown in Table 1. The total efficiency is low due to the absorption of radiated power in the lossy properties of colon tissue.

Table 1: Gain and total efficiency of the MIMO antennas.

MIMO antennas	Gain	Total efficiency
Antenna 1	-15.19 dB	-20.15 dB
Antenna 2	-15.73 dB	-20.29 dB

4.2 Design and analysis of on-body MIMO antennas using the RT Duroid substrate

The substrate material with high permittivity and small thickness can considerably reduce the dimensions of an antenna [38]. Therefore, a 0.635 mm thick RT Duroid substrate ($\epsilon_r = 10.2$ and $\tan\delta = 0.0022$) is used to design the on-body MIMO antennas.

4.2.1 Geometry of the MIMO antennas structure

The printed monopole antennas on the FR-4 substrate are optimized for the high permittivity RT Duroid substrate. The new geometry of proposed printed monopole antennas is shown in Fig. 25. The size of antenna structure is reduced to 45 mm × 45 mm due to higher permittivity of RT Duroid than the FR-4 substrate. The printed monopole antennas are placed orthogonal to each other for dual polarization. Moreover, the common ground plane of 4 mm width is used to improve the impedance matching level at 433 MHz.

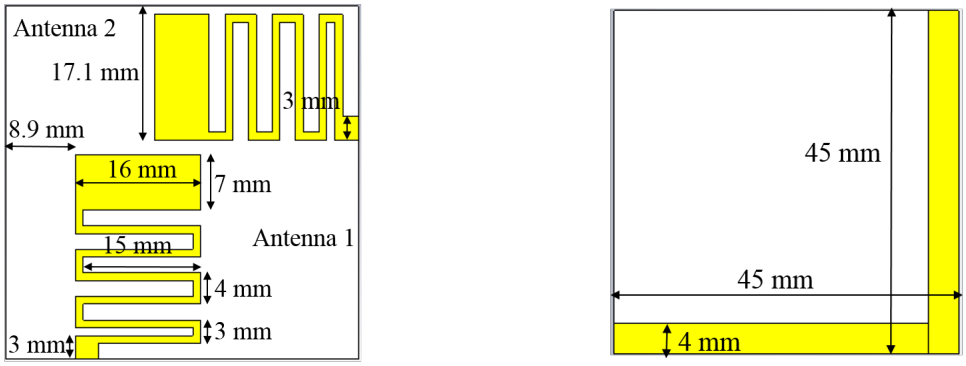

Fig. 25: Geometry of the MIMO antennas structure using the RT Duroid substrate: (a) top view; (b) bottom view.

4.2.2 Simulation set-up and results

In the simulation set-up, antenna structure is facing towards the colon tissue as shown in Fig. 26. The motivation of this simulation set-up is to increase the dielectric loading effect on MIMO antennas as they are facing towards high permittivity colon tissue instead of free space. Thus, considerable miniaturization of MIMO antennas is achieved at 433 MHz.

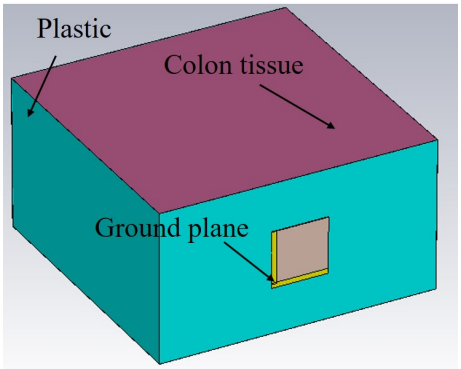

Fig. 26: Antenna structure facing towards the body phantom

Moreover, 1 mm air gap is considered between the antenna structure and body phantom to accommodate the spacing due to probe feed connectors. In the measurement set-up, the ground pins of probe feed connectors will face towards free space instead of body phantom and thus reduce the air gap as compared to SMA connectors. The simulated reflection coefficients of antenna 1 and antenna 2 are shown in Fig. 27(a). The reflection coefficients of antenna 1 and antenna 2 at 433 MHz are -12.29 dB and -13.49 dB respectively. Moreover, the MIMO antennas have shown -10 dB impedance bandwidth of 47 MHz (418-465 MHz).

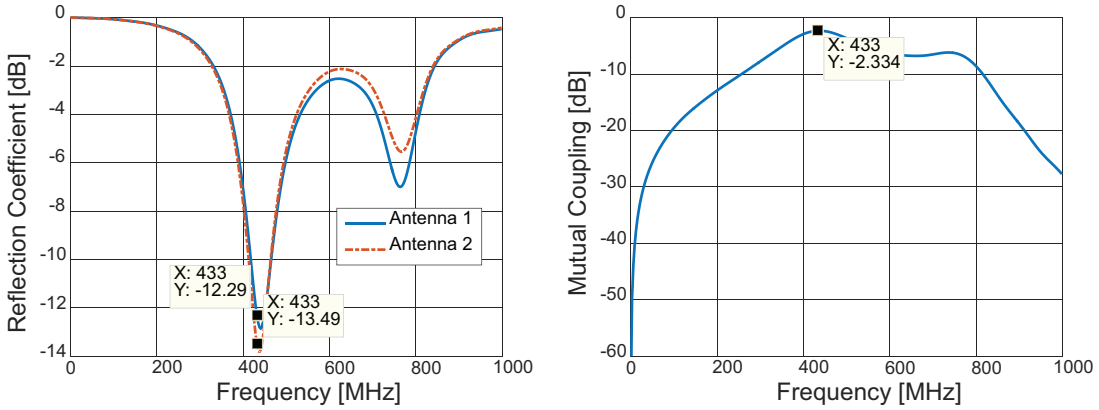

(a) (b)

Fig. 27: Simulated results of MIMO antennas using the RT Duroid substrate: (a) reflection coefficients; (b) mutual coupling.

The mutual coupling between MIMO antennas is shown in Fig. 27(b). It can be seen that the mutual coupling is high at 433 MHz. Thus, the colon tissue has insignificant impact to absorb electric current on the common ground plane when the MIMO antennas are facing towards the body phantom.

4.2.3 Geometry of the antenna structure with separate ground planes

The high mutual coupling can reduce the efficiency of MIMO antennas. Therefore, separate ground plane is proposed for each printed monopole antenna to prevent the flow of electric current between the MIMO antennas. Thus, considerable decrease in the mutual coupling is possible even when the MIMO antennas are facing towards the body phantom.

The new geometry of printed monopole antennas is shown in Fig. 28. The size of antenna structure is 65 mm $\times$ 65 mm and the width of each ground plane is 4 mm. The size of antenna structure has increased as compared to when the ground plane is common for MIMO antennas. Moreover, the number of meander lines have optimized to resonate the MIMO antennas at 433 MHz. The width of each meander line is 1 mm and the ground planes are separated from the substrate edge by 5 mm.

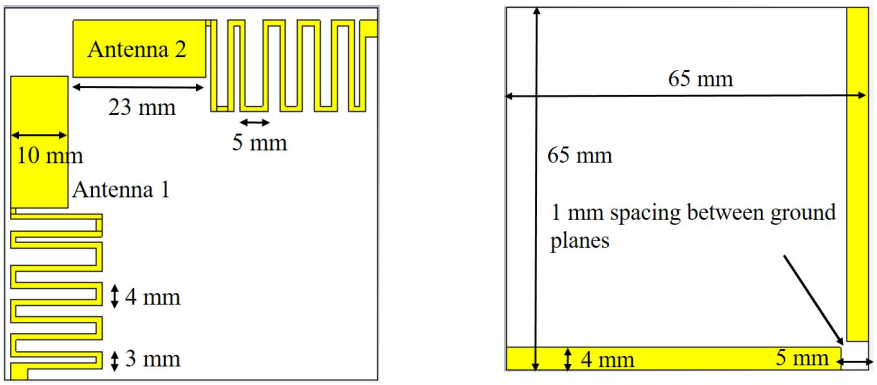

(a) (b)

Fig. 28: Geometry of MIMO antenna with separate ground planes using the RT Duroid substrate: (a) top view; (b) bottom view.

The simulated reflection coefficients of MIMO antennas are shown in Fig. 29(a). The MIMO antennas are well matched at 433 MHz. The -10 dB impedance bandwidth of antenna 1 and antenna 2 is 41 MHz (411-452 MHz).

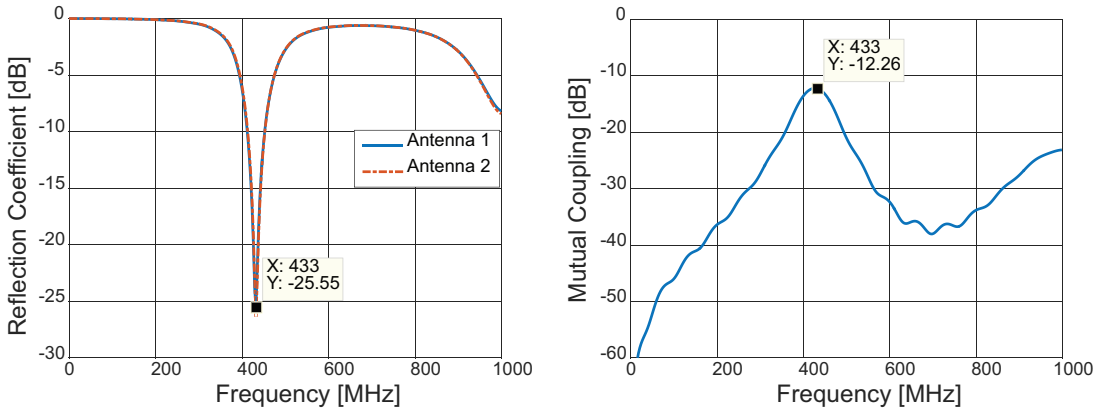

(a) (b)

Fig. 29: Simulated results of MIMO antennas with separate ground planes using the RT Duroid substrate: (a) reflection coefficients; (b) mutual coupling.

The mutual coupling between MIMO antennas is shown in Fig. 29(b). It is observed that the mutual coupling is less than -10 dB over a wide range of frequencies. The simulated mutual coupling ($|S_{21}|=|S_{12}|$) is -12.26 dB at 433 MHz. Thus, the separate ground planes can reduce the mutual coupling significantly when the MIMO antennas are facing towards the body phantom. However, the antenna dimensions increases with separate ground planes and more meander lines are required for considerable miniaturization.

The simulated gain and total efficiency are shown in Table 2. The lossy properties of colon tissues have the deteriorating impacts on the efficiency of MIMO antennas.

Table 2: Gain and total efficiency of the MIMO antennas with separate ground planes.

MIMO antennas	Gain	Total efficiency
Antenna 1	-19.89 dB	-22.45 dB
Antenna 2	-19.13 dB	-22.30 dB

4.3 Design and analysis of on-body MIMO antennas using the flexible substrate

The flexible substrate can be conformed around the human body and thus offers comfort for the patients. In this section, a 0.55 mm thick flexible substrate ($\epsilon = 11$ and $\tan\delta = 0.0003$) is used in the design of dual polarized MIMO antennas for an on-body receiver of a WCE system.

4.3.1 Geometry of the antenna structure

The MIMO antennas designed using the RT Duroid are now optimized for the flexible substrate. The new geometry of MIMO antennas is shown in Fig. 30.

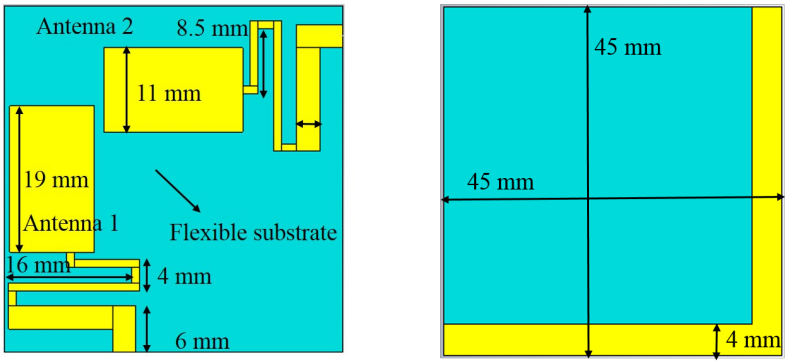

(a) (b)

Fig. 30: Geometry of the MIMO antennas using the flexible substrate: (a) top view; (b) bottom view.

4.3.2 Simulation set-up and results

In the simulation set-up, the antenna structure is facing towards the body phantom with 1 mm air gap due to probe feed connectors. The simulated reflection coefficients of antenna 1 and antenna 2 at 433 MHz are -9.8 dB and -10.01 dB respectively

as shown in Fig. 31(a). The simulated mutual coupling between the MIMO antennas at 433 MHz is -3.726 dB as shown in Fig. 31(b). The mutual coupling can be reduced further with separate ground planes. However, the separate ground planes are not used for flexible substrate as they increase the size of antenna structure.

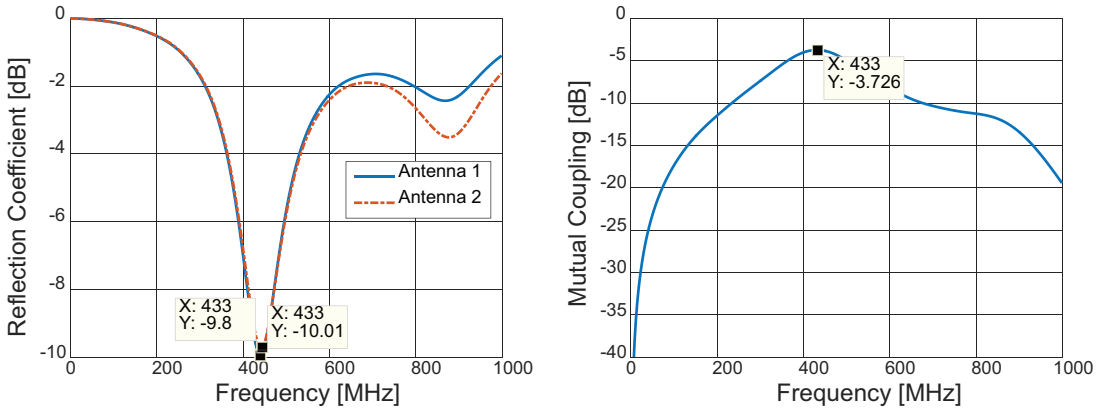

(a) (b)

Fig. 31: Simulated results of MIMO antennas using the flexible substrate: (a) reflection coefficients; (b) mutual coupling.

The gain and total efficiency of MIMO antennas are shown in Table 3. The lossy properties of colon tissue absorbs the power radiated from MIMO antennas and decrease the total efficiency.

Table 3: Gain and total efficiency of the MIMO antennas using the flexible substrate.

MIMO antennas	Gain	Total efficiency
Antenna 1	-28.56 dB	-22.43 dB
Antenna 2	-29.55 dB	-23.36 dB

4.4 Chapter summary

In this chapter, the design and analysis of MIMO antennas were presented for the on-body receiver of a WCE system. Two dual polarized printed monopole antennas were designed using the flat and flexible substrates. The FR-4 and RT Duroid substrates were used as flat substrates and a 0.5 mm thick material was used as flexible substrate. The performance of designed antenna structures was characterized on the body phantom with colon tissue properties at 433 MHz.

The summarized simulated results are described in Table 4. It is observed that the antenna size becomes compact by using the high permittivity substrate, such as RT Duroid and flexible. The total efficiency of an on-body increases on the large and low permittivity substrate. Therefore, the MIMO antennas using the FR-4

Table 4: Simulated results

Substrate	**Antenna size**	**Total efficeincy**
FR-4	87 mm × 87 mm	Ant 1= -20.15 dB
ϵ_r=4.3	Common ground planne	Ant 2= -20.29 dB
RT Duroid	45 mm × 45 mm	Ant 1= -27.35 dB
ϵ_r=10.2	Common ground planne	Ant 2= -28.26 dB
RT Duroid	65 mm × 65 mm	Ant 1= -22.45 dB
ϵ_r=10.2	Separate ground planne	Ant 2= -22.30 dB
Flexible	45 mm × 45 mm	Ant 1= -22.43 dB
ϵ_r=11	Common ground planne	Ant 2= -23.36 dB

substrate have better total efficiency than the RT Duroid and flexible substrates. The separate ground planes can be used to reduce the mutual coupling between the MIMO antennas. However, the antenna size increases and minimization techniques, such as meander lines are required for the compact dimensions.

5 Measurement Results of the On-Body MIMO Antennas

This chapter presents the fabrication process and measurement results of the on-body MIMO antennas. The measurements are performed on the liquid phantom mimicking colon tissue at 433 MHz. The E5063A Agilent Vector Network Analyzer (VNA) is used to perform the reflection coefficient and mutual coupling measurements of the fabricated antenna structures.

The chapter is organized as follows: Section 5.1 discusses the liquid phantom formulation with the colon tissue properties at 433 MHz. In Section 5.2, the fabrication process and measurement results of the on-body antenna using the FR-4 substrate are presented. The Section 5.3 describes the measurement results using the RT Duroid substrate. In Section 5.4, the fabricated antenna structure using the flexible substrate is measured on the liquid phantom. The measurement results on the human body are described in Section 5.5. Lastly, the chapter summary is presented in Section 5.4.

5.1 Liquid phantom formulation

In order to verify the simulated results, the fabricated on-body antenna structures are measured in the similar environment. For this purpose, a liquid mimicking colon tissue properties is developed in the plastic container. The liquid is formulated by mixing salted water and TrintonX-100. The transmission line propagation method is used to measure the dielectric properties of the liquid with the HP 8720C Network Analyzer and 85070A dielectric probe kit. The measured values of permittivity and conductivity are shown in Table. 5.

Table 5: Recipe of the liquid phantom mimicking colon tissue.

Frequency	Recipe	Target Values	Measured Values
433 MHz	Salted water 79 % (7.85 g/liter) TritonX-100 21 %	$\epsilon = 62.01$; $\sigma = 0.87$	$\epsilon = 61.38$; $\sigma = 0.89$

5.2 On-body receiving antennas using the FR-4 substrate

5.2.1 Fabrication process

The designed antenna structure using the FR-4 substrate is fabricated with the photo-lithography chemical etching process. In first step of the etching process, the substrate material is cut according to the designed antenna dimensions. Then, a photo mask containing the pattern of the antenna structure is placed on the substrate as shown in Fig. 32(a). In the next step, the substrate is exposed to ultraviolet (UV) light for 6 minutes as shown in Fig. 32(b). The opaque region on the photo mask blocks the UV light and becomes polymerized on the substrate. Lastly, the substrate is dipped in the solvent called as developer. The developer dissolves the

unexposed region while polymerized region containing the antenna pattern remains on the substrate. The same procedure is used for fabricating the ground plane.

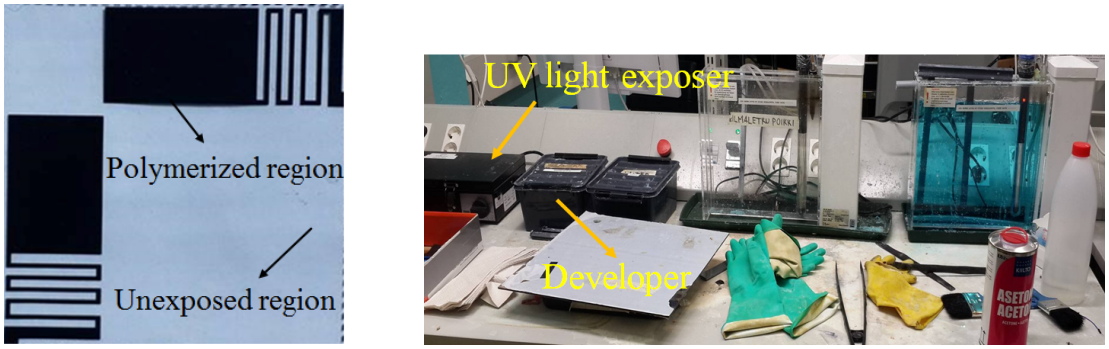

(a) (b)

Fig. 32: Photo-lithography chemical etching process: (a) photo mask of the antenna pattern from top; (b) fabrication set-up.

The fabricated prototype is shown in Fig. 33. A SMA connector is soldered to each printed monopole antenna for feeding through the coaxial cables.

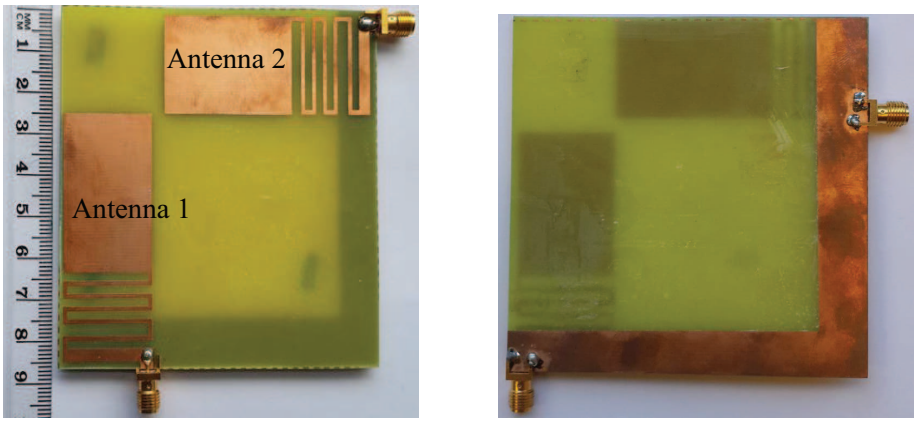

(a) (b)

Fig. 33: Fabricated MIMO antennas using the FR-4 substrate: (a) top view; (b) bottom view.

5.2.2 Measurements on the liquid phantom

The fabricated MIMO antennas are measured on the liquid phantom to characterize their performance in terms of reflection coefficients and mutual coupling. The measurements are performed using the E5063A Agilent Vector Network Analyzer

(VNA). The measurement set-up is illustrated in Fig. 34.

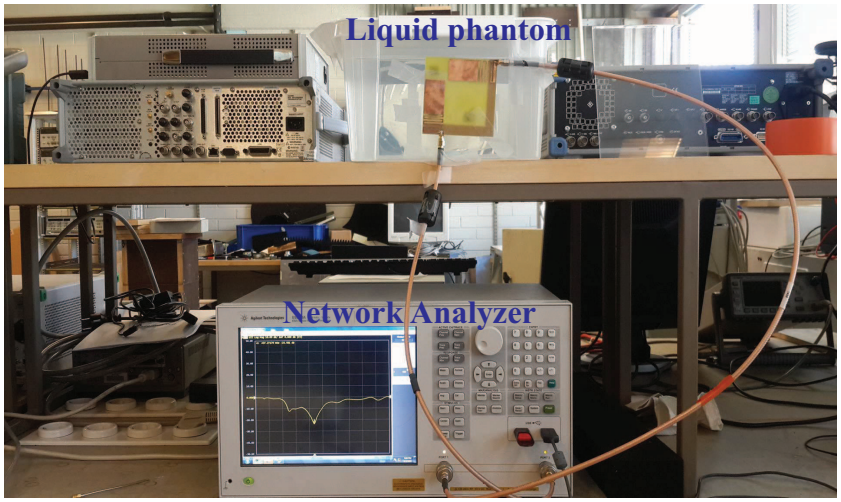

Fig. 34: Measurement set-up of MIMO antennas on the liquid phantom.

It is worth mentioning that the antenna structure is approximately 2 mm away from the liquid phantom. The air gap is due to the ground pins of a SMA connector as shown in Fig. 35. Thus, the measurement set-up has validated the simulation environment where the air gap was considered between the antenna structure and body phantom.

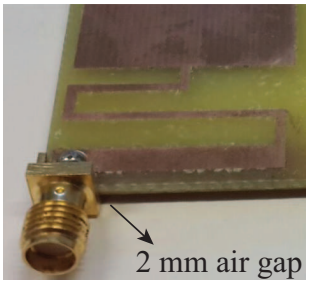

Fig. 35: 2 mm air gap due to the ground pins of a SMA connector.

The comparison between simulated and measured reflection coefficients of the MIMO antennas are shown in Fig. 36. The measured reflection coefficients of antenna 1 and antenna 2 are shifted towards lower frequencies by 24 MHz and 59 MHz respectively. The shift in reflection coefficients is due to possible uncertainties in the fabrication and measurements process. For instance, the antenna structure is attached on the liquid phantom with the help of plastic tape. Therefore, it is difficult to maintain the uniform 2 mm distance between the antenna structure and

liquid phantom due to imbalance force by plastic tapes. The dielectric loading effect increases on the antenna which is closer to the liquid phantom and thus detunes more towards lower frequencies. However, the MIMO antennas are still maintaining good level of matching at 433 MHz.

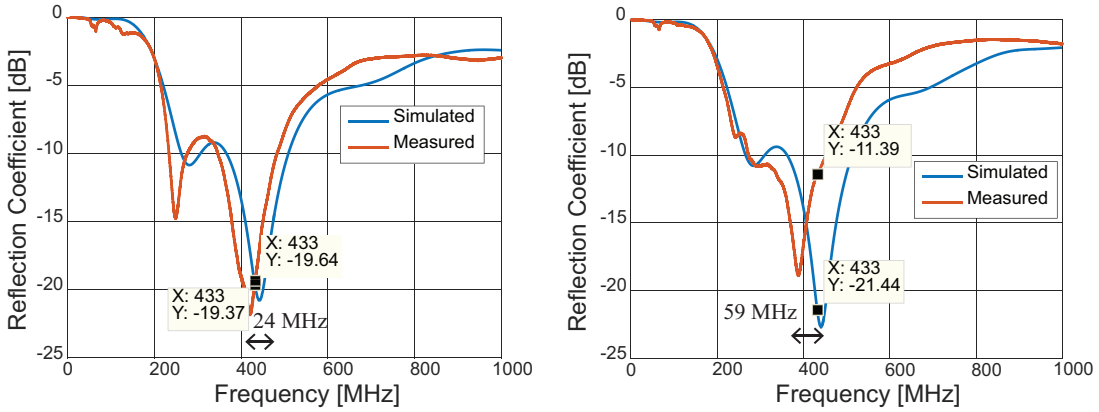

(a) (b)

Fig. 36: Comparison between simulated and measured reflection coefficients of MIMO antennas using the FR-4 substrate: (a) antenna 1; (b) antenna 2.

The measured and simulated mutual couplings ($|S_{21}|$=$|S_{12}|$) between the MIMO antennas are compared in Fig. 37. The mutual coupling mainly depends on the antenna distance from the liquid phantom The 3 dB difference is observed at 433 MHz between the measured and simulated results of mutual coupling.

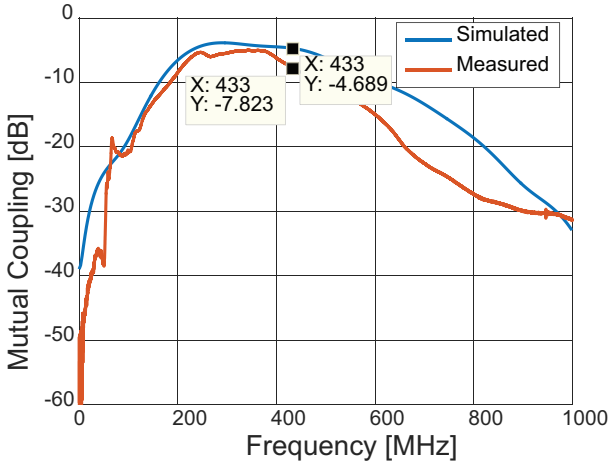

Fig. 37: Simulated and measured mutual coupling between MIMO antennas on the liquid phantom.

5.3 Measurements of the on-body MIMO antennas using the RT Duroid substrate

The prototype of fabricated MIMO antennas using the RT Duroid ($\epsilon_r = 10.2$ and $\tan\delta = 0.0022$) is shown in Fig. 38(a). The photo-lithography chemical etching process is used for fabricating the antenna structure. The ground plane is common for both printed monopole antennas as shown in Fig. 38(b). A probe feed connector is soldered to each printed monopole antenna from the common ground plane.

(a) (b)

Fig. 38: Fabricated MIMO antennas using the RT Duroid substrate: (a) top view; (b) bottom view.

In the measurement set-up, the antenna structure is facing towards the liquid phantom as shown in Fig. 39. The plastic tapes are used to attach antenna structure on the wall of liquid phantom. The soldered pins of both probe feed connectors are keeping the antenna structure approximately 1 mm away from the liquid phantom. Thus, the measurement set-up has validated the simulation environment where 1 mm air gap was considered between the antenna structure and body phantom as presented in Section 4.2.2.

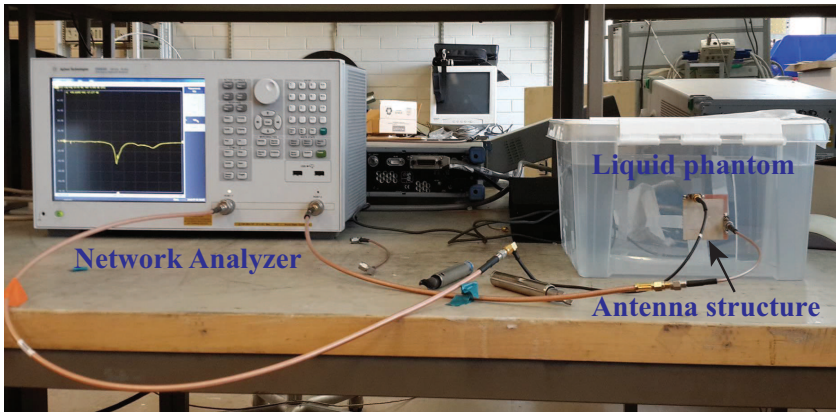

Fig. 39: Measurement set-up of MIMO antennas using the RT Duroid substrate.

The simulated and measured reflection coefficients of antenna 1 are in good agreement of matching as shown in Fig. 40(a). However, the measured reflection coefficient of antenna 2 are slightly shifted towards higher frequencies by 28 MHz as shown in Fig. 40(b). The frequency shift is due to non uniform 1 mm gap between the antenna 2 and liquid phantom.

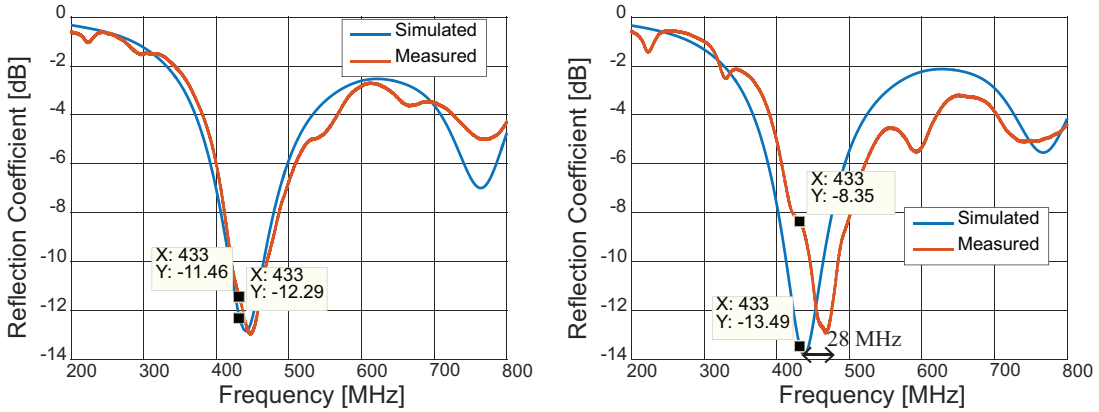

(a) (b)

Fig. 40: Comparison between simulated and measured reflection coefficients of MIMO antennas using the RT Duroid substrate: (a) antenna 1; (b) antenna 2.

The comparison between simulated and measured mutual coupling ($|S_{21}|$=$|S_{12}|$) between the MIMO antennas is shown in Fig. 41. At 433 MHz, the measured mutual coupling is found to be approximately 2 dB lower than the simulated mutual coupling.

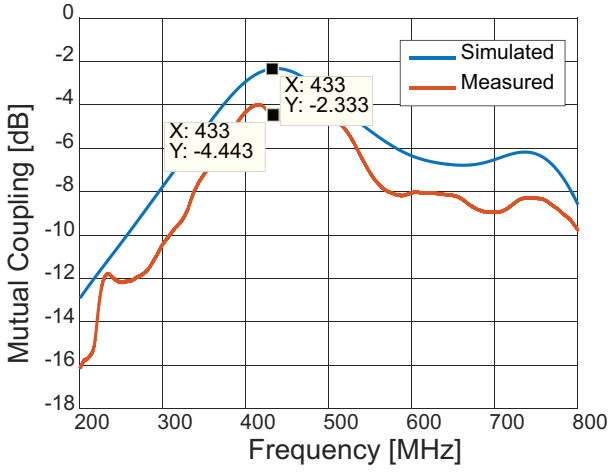

Fig. 41: Comparison between simulated and measured mutual coupling of MIMO antennas using the RT Duroid substrate.

In order to reduce the mutual coupling between MIMO antennas, the antenna structure with separate ground planes is fabricated. The fabricated MIMO antennas are shown in Fig. 42(a). The ground plane of printed monopole antennas are separated by 5 mm from the edge as shown in Fig. 42(b). In the measurement set-up, the antenna structure is facing towards liquid phantom with 1 mm air gap due to soldered pins of SMA connectors.

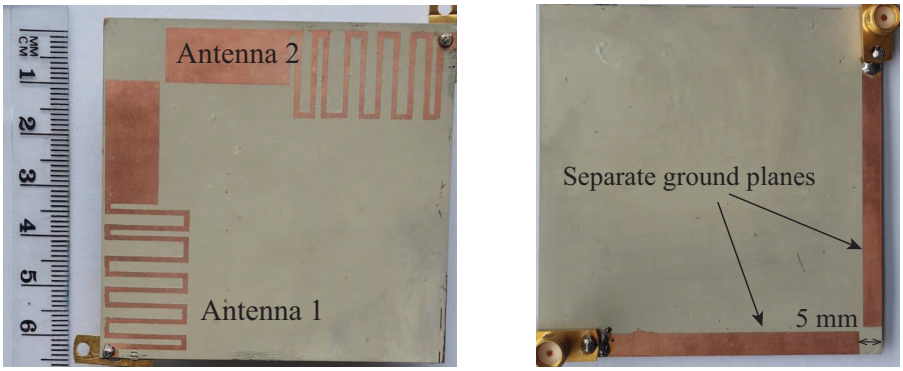

(a) (b)

Fig. 42: Fabricated MIMO antennas with separate ground planes using the RT Duroid substrate: (a) top view; (b) bottom view.

The simulated and measured reflection coefficients of MIMO antennas are compared in Fig. 43. A good agreement between the simulated and measured reflection coefficients has been achieved. However, the measured reflection coefficients of antenna 1 and antenna 2 are shifted by 16 MHz and 19 MHz respectively. The frequency shift is due to uncertainties in keeping an uniform 1 mm air gap between the antenna structure and liquid phantom.

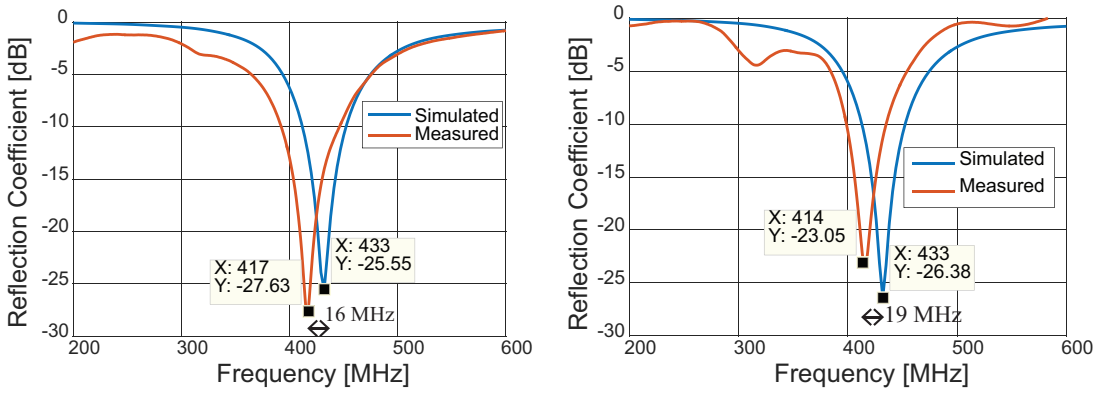

(a) (b)

Fig. 43: Comparison between simulated and measured reflection coefficients of MIMO with separate ground planes using the RT Duroid substrate: (a) antenna 1; (b) antenna 2.

The measured and simulated mutual coupling ($|S_{21}|=|S_{12}|$) between MIMO antennas are compared in Fig. 44. At 433 MHz, the measured mutual coupling is -16.22 dB. Thus, the separate ground planes can significantly reduce the mutual coupling when the MIMO antennas are facing towards the liquid phantom.

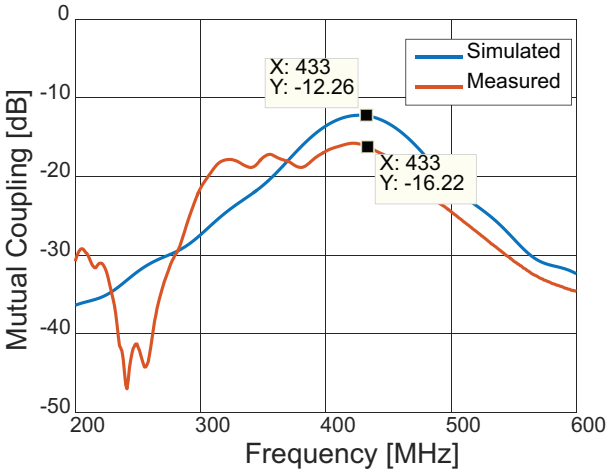

Fig. 44: Comparison between simulated and measured mutual coupling between MIMO antennas with separate ground planes using the RT Duroid substrate.

5.4 Measurements of the on-body MIMO antennas using the flexible substrate

The prototype of fabricated MIMO antennas using the flexible substrate is shown in Fig. 45(a). For feeding the MIMO antennas, two SMA connectors are soldered through the common ground plane as shown in Fig. 45(b).

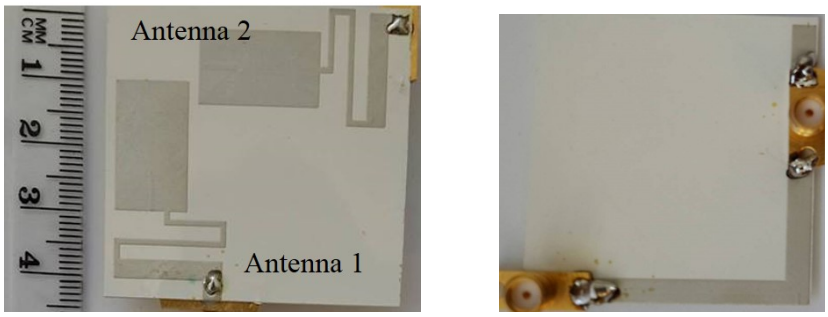

(a) (b)

Fig. 45: Fabricated on-body MIMO antennas using the flexible substrate: (a) top view; (b) bottom view.

In the measurement set-up, antenna structure is facing towards the liquid phantom as shown in Fig. 46. The soldered pins of probe feed connectors are keeping the antenna structure approximately 1 mm away from the wall of liquid phantom.

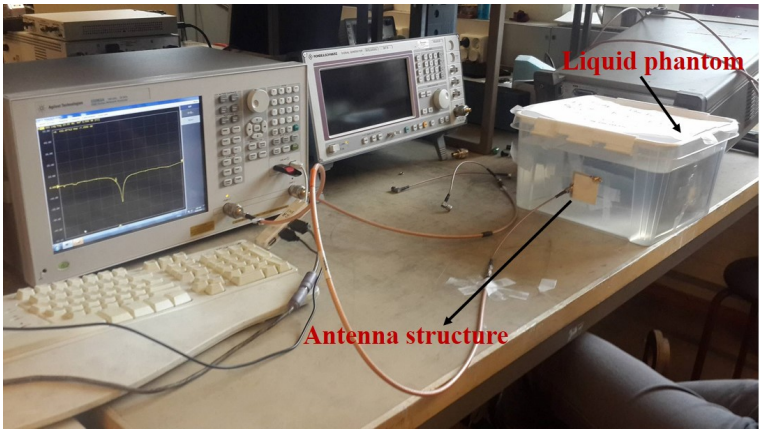

Fig. 46: Measurement set-up of MIMO antennas using the flexible substrate.

The comparison between simulated and measured reflection coefficients are shown in Fig. 47. It can be seen that the simulated and measured reflection coefficients of antenna 1 are in good agreement of matching. However, 3 dB difference in matching level is observed between the simulated and measured reflection coefficients of antenna 2 at 433 MHz.

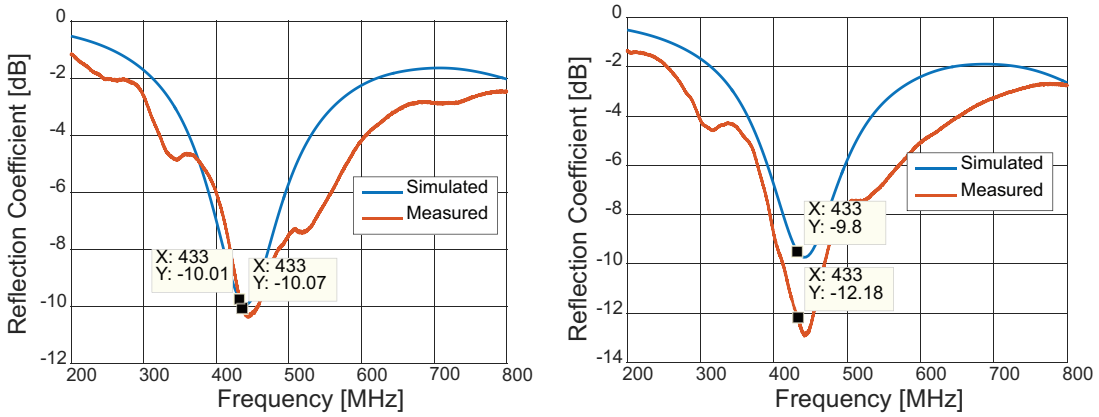

(a) (b)

Fig. 47: Comparison between simulated and measured reflection coefficients of MIMO using the flexible substrate: (a) antenna 1; (b) antenna 2.

The simulated and measured mutual coupling ($|S_{21}|$=$|S_{12}|$) between the MIMO antennas is shown in Fig. 48. The measured mutual coupling is found to be 2 dB lower than the simulated mutual coupling.

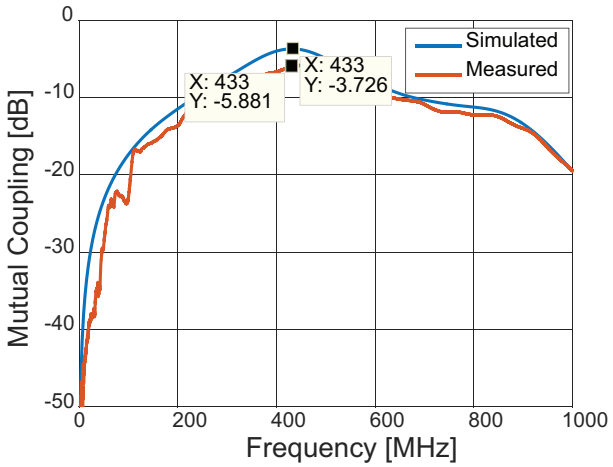

Fig. 48: Simulated and measured mutual coupling on the liquid phantom using flexible substrate.

5.5 Measurements on the human body

In the practical application of WCE, the on-body antenna will be attached on the patient's abdomen. Therefore, the antenna structure which is fabricated using the FR-4 substrate is selected for performing measurements on the human body as shown in Fig. 49. The motivation of this measurement set-up is to study the impacts of real body tissues on the performance of designed MIMO antennas.

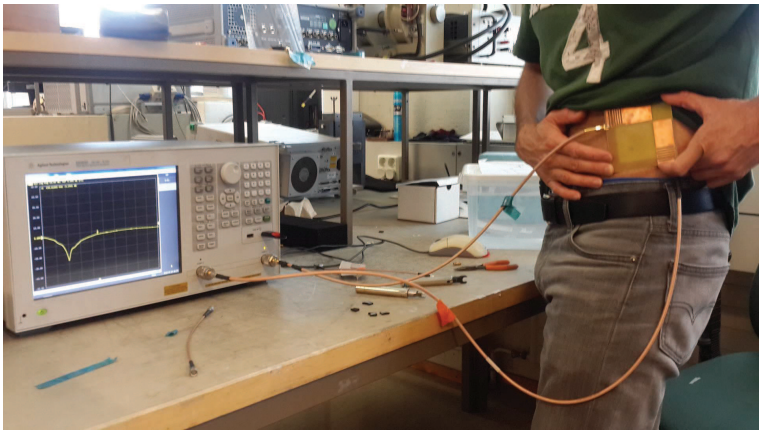

Fig. 49: Measurements on the human body using the FR-4 substrate.

Fig. 50 illustrates the comparison between measured reflection coefficients on the human body and liquid phantom. It is found that the MIMO antennas are detuned to much lower frequencies on the human body as compared to liquid phantom. The

frequency shift for antenna 1 and antenna 2 is 244 MHz and 202 MHz respectively.

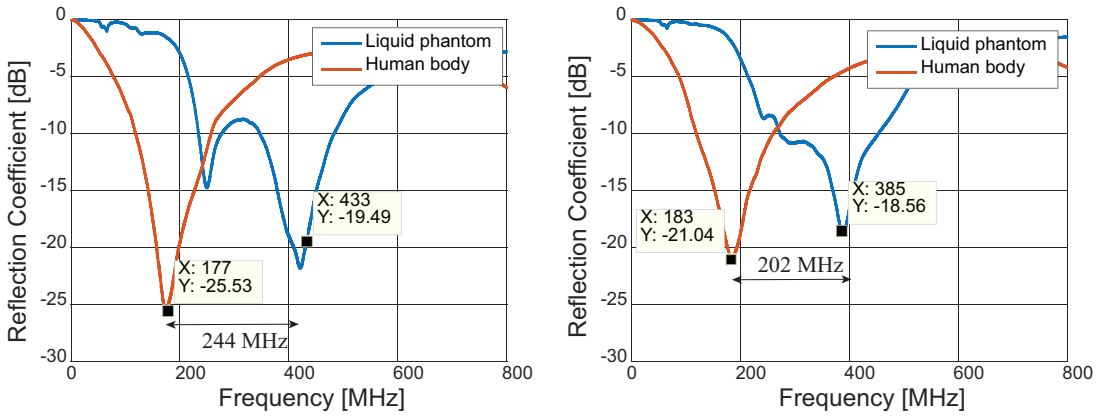

(a) (b)

Fig. 50: Comparison between measured reflection coefficients on the human body and liquid phantom: (a) antenna 1; (b) antenna 2.

The frequency shifts are due to more dielectric loading effect from the human body than liquid phantom. The antenna structure on the human body is completely attached with the skin due to its soft and conformal nature. In contrast, antenna structure is approximately 2 mm away from colon tissue on the liquid phantom. Therefore, the dielectric loading effect increases on the human body and MIMO antennas detune to low frequencies.

In Fig. 51, mutual coupling on the human body and liquid phantom are compared. The mutual coupling has decreased significantly on the human body as the ground plane is completely attached with the skin.

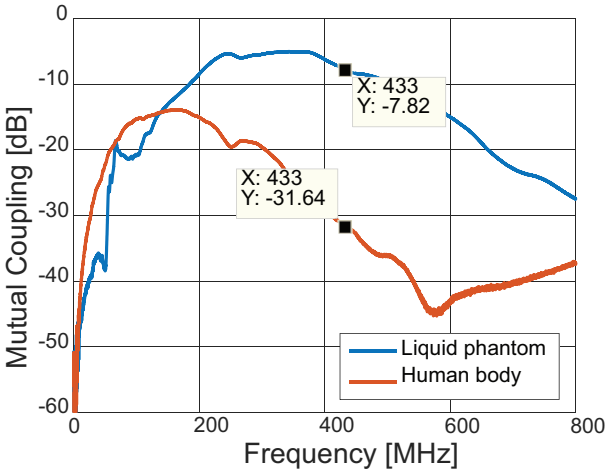

Fig. 51: Measured mutual coupling on the liquid phantom and human body.

The skin tissue absorbs electric current on the common ground plane and reduce its flow between antenna ports. However, antenna structure on the liquid phantom is not completely attached with the colon tissue due to 2 mm air gap. Thus, the impact of colon tissue is lower than human body for reducing mutual coupling between the MIMO antennas.

It is important to mention that the on-body MIMO antennas in this chapter are specifically designed for the colon tissue only due to our available measurement set-up in the laboratory.

5.6 Chapter summary

The measurement results of on-body MIMO antennas were presented for a WCE system. The antennas were fabricated using the FR-4, RT Duroid and flexible substrates. The photo-lithography chemical etching process was used for fabricating the antenna structures. The liquid phantom with colon tissue properties at 433 MHz was used to characterize the performance of MIMO antennas in terms of reflection coefficient and mutual coupling. A good agreement of matching was observed between the simulated and measured results. However, the frequency shifts in measured reflection coefficients were found due to uncertainties in the fabrication and measurement process.

The mutual coupling between MIMO antennas was also measured and compared with the simulated results. The measured mutual coupling for all designed on-body MIMO antennas was found to be lower than the simulated results. Moreover, separate ground planes were used to reduce the mutual coupling between MIMO antennas. Lastly, antenna structure with the FR-4 substrate was measured on the human body. It was observed that the MIMO antennas on the human body resonate at lower frequencies than the liquid phantom.

6 Conclusions and Future works

In this master thesis, the antenna solutions were analzyed for a wireless capsule endoscopy system. The dual polarized MIMO antennas were designed and optimized for the in-body capsule transmitter and on-body receiver at 433 MHz. The colon tissue properties at 433 MHz were used to characterize the performance of designed MIMO antennas. The simulated results of on-body antennas were validated by performing measurements on the liquid phantom mimicking colon tissue.

Two conformal loop antennas were designed for the in-body capsule transmitter. One loop antenna was conformed around the inner surface of capsule shell, while the second loop antenna utilized the outer surface. The inner shell loop antenna was designed with meander lines and the outer shell loop antenna was designed with rectangular patches. The simulated results inside the body phantom showed that the -10 dB bandwidth of inner shell loop antenna was narrow as compared to the outer shell loop antenna due to meander lines and compact size. The mutual coupling between MIMO antennas was less than -20 dB over a wide range of frequencies. Moreover, the performance of MIMO antennas was evaluated with different orientations of capsule inside the body phantom. The MIMO antennas were found robust against the detuning and maintained good level of matching at 433 MHz.

For on-body receiver, two orthogonal printed monopole antennas were designed using the flat and flexible substrates. The FR-4 and RT Duroid were used as flat substrates, while a 0.55 mm thick material was used as flexible substrate. The motivation of using different substrates was to study their impacts on antenna size, -10 dB impedance bandwidth and efficiency. The on-body MIMO antennas using the high permittivity RT Duroid ($\epsilon = 10.2$) and flexible ($\epsilon = 11$) substrates were more compact than the low permittivity FR-4 ($\epsilon = 4.3$) substrate. However, the -10 dB impedance bandwidth and efficiency were decreased using the high permittivity substrates. The dielectric loading effect was increased when the MIMO antennas on the body phantom were facing towards colon tissue instead of free space. Thus, this phenomena was used miniaturize the on-body MIMO antennas at 433 MHz.

The impact of colon tissue on the mutual coupling between MIMO antennas was discussed. It was found that the mutual coupling depends on the absorption of electric current which is flowing between antenna ports on the common ground plane. The mutual coupling was high when the MIMO antennas on the body phantom were facing towards colon tissue instead of free space. Therefore, separate ground planes were used to prevent the flow of electric current between antenna ports. The separate ground planes of MIMO antennas reduced the mutual coupling less than -10 dB over a wide range of frequencies.

The on-body MIMO antennas were fabricated using the FR-4, RT Duroid and flexible substrates. The photo-lithography chemical etching process was used for fabricating the antenna structures. The measurements were performed on the liquid phantom mimicking colon tissue. It was found that the measured and simulated reflection coefficient were in good agreement of matching. However, the frequency shift in reflection coefficients was observed due to possible uncertainties in the fabrication and measurement process.

The MIMO antennas using FR-4 substrate were measured on the human body to compare their performance with the measured results on the liquid phantom. The antenna structure was completely attached with the skin due to its soft and conformal nature. However, the SMA connectors were keeping the antenna structure approximately 2 mm away from the liquid phantom. Thus, the reflection coefficients of MIMO antennas were shifted towards lower frequencies on the human body due to more dielectric loading effect than liquid phantom. Moreover, the mutual coupling between MIMO antennas was decreased significantly on the human body as the common ground plane was attached with the skin without any air gap.

The future works include fabrication of the dual polarized MIMO antennas for the in-body capsule transmitter and their measurements inside the liquid phantom. In the next phase, the path loss analysis will be measured between the in-body capsule and on-body receiver at 433 MHz.

References

[1] A. Rosen, M. A. Stuchly, and A. V. Vorst, "Applications of RF/microwaves in medicine," *IEEE Transactions on Microwave Theory and Techniques*, vol. 50, no. 3, pp. 963–974, Mar 2002.

[2] H. Wang, D. Chen, M. Q. H. Meng, C. Hu, and Z. Liu, "Robust abnormal wireless capsule endoscopy frames detection based on least squared density ratio algorithm," in *IEEE International Conference on Information and Automation (ICIA)*, June 2011, pp. 324–328.

[3] D. Chen, M. Q. H. Meng, H. Wang, C. Hu, and Z. Liu, "A novel strategy to label abnormalities for wireless capsule endoscopy frames sequence," in *IEEE International Conference on Information and Automation (ICIA)*, June 2011, pp. 379–383.

[4] T. Castel, P. Van Torre, E. Tanghe, S. Agneessens, G. Vermeeren, W. Joseph, and H. Rogier, "Improved reception of in-body signals by means of a wearable multi-antenna system," *International Journal of Antennas and Propagation, Article ID 328375*, vol. 2013, pp. 1–9, 2013.

[5] C. Kim and S. Nooshabadi, "Analysis of a DTR UWB receiver with multiple antennas for high-data rate wireless biotelemetry," in *IEEE Biomedical Circuits and Systems Conference*, Nov 2009, pp. 145–148.

[6] J. Thoné, S. Radiom, D. Turgis, R. Carta, G. Gielen, and R. Puers, "Design of a 2 Mbps FSK near-field transmitter for wireless capsule endoscopy," *Sensors and Actuators A-Physical*, vol. 156, no. 1, pp. 43–48, 2009.

[7] K. Takizawa and K. Hamaguchi, "Low-complexity video encoding method for wireless image transmission in capsule endoscope," in *Annual International Conference of the IEEE Engineering in Medicine and Biology*, Aug 2010, pp. 3479–3482.

[8] K. M. S. Thotahewa, J. M. Redouté, and M. R. Yuce, "A UWB wireless capsule endoscopy device," in *36th Annual International Conference of the IEEE Engineering in Medicine and Biology Society*, Aug 2014, pp. 6977–6980.

[9] S. Stoa, R. Chávez-Santiago, and I. Balasingham, "An ultra wideband communication channel model for capsule endoscopy," in *3rd International Symposium on Applied Sciences in Biomedical and Communication Technologies (ISABEL 2010)*, Nov 2010, pp. 1–5.

[10] R. Chávez-Santiago, J. Wang, and I. Balasingham, "The ultra wideband capsule endoscope," in *IEEE International Conference on Ultra-Wideband (ICUWB)*, Sept 2013, pp. 72–78.

[11] P. A. Floor, R. Chávez-Santiago, S. Brovoll, Aardal, J. Bergsland, O. J. H. N. Grymyr, P. S. Halvorsen, R. Palomar, D. Plettemeier, S. E. Hamran, T. A. Ramstad, and I. Balasingham, "In-body to on-body ultrawideband propagation model derived from measurements in living animals," *IEEE Journal of Biomedical and Health Informatics*, vol. 19, no. 3, pp. 938–948, May 2015.

[12] A. Khaleghi and I. Balasingham, "Wireless communication link for capsule endoscope at 600 MHz," in *37th Annual International Conference of the IEEE Engineering in Medicine and Biology Society (EMBC)*, Aug 2015, pp. 4081–4084.

[13] P. Quinlan, P. Crowley, M. Chanca, S. Hudson, B. Hunt, K. Mulvaney, G. Retz, C. E. O'Sullivan, and P. Walsh, "A multimode 0.3-200-kb/s transceiver for the 433/868/915-mhz bands in 0.25- mu/m CMOS," *IEEE Journal of Solid-State Circuits*, vol. 39, no. 12, pp. 2297–2310, Dec 2004.

[14] Y. Shimizu, D. Anzai, and J. Wang, "Performance evaluation on transmit polarization diversity for implant UWB-IR communications," in *9th International Symposium on Medical Information and Communication Technology (ISMICT)*, March 2015, pp. 175–179.

[15] Y. Shimizu, T. Furukawa, D. Anzai, and J. Wang, "Performance comparison between UWB-IR and MB-OFDM with transmit diversity in implant communications," in *37th Annual International Conference of the IEEE Engineering in Medicine and Biology Society (EMBC)*, Aug 2015, pp. 5469–5472.

[16] H. B. Li, K. i. Takizawa, B. Zhen, and R. Kohno, "Body Area Network and Its Standardization at IEEE 802.15. MBAN," in *16th IST Mobile and Wireless Communications Summit*, July 2007, pp. 1–5.

[17] I. Guideline, "Guidelines for limiting exposure to time-varying electric, magnetic, and electromagnetic fields (up to 300 GHz)," *Health Phys*, vol. 74, no. 4, pp. 494–522, 1998.

[18] Z. N. Chen, *Antennas for portable devices*. John Wiley & Sons, 2007.

[19] K. Y. Yazdandoost, "UWB loop antenna for in-body wireless body area network," in *Antennas and Propagation (EuCAP), 2013 7th European Conference on*, April 2013, pp. 1138–1141.

[20] [Online]. Available: http://niremf.ifac.cnr.it/tissprop/htmlclie/htmlclie.php

[21] A. K. Skrivervik, "Implantable antennas: The challenge of efficiency," in *7th European Conference on Antennas and Propagation (EuCAP)*, April 2013, pp. 3627–3631.

[22] W. Liu, S. Chen, and C. Wu, "Implantable broadband circular stacked PIFA antenna for biotelemetry communication," *Journal of Electromagnetic Waves and Applications*, vol. 22, no. 13, pp. 1791–1800, 2008.

[23] J. Kim and Y. Rahmat-Samii, "Implanted antennas inside a human body: simulations, designs, and characterizations," *IEEE Transactions on Microwave Theory and Techniques*, vol. 52, no. 8, pp. 1934–1943, Aug 2004.

[24] T. Karacolak, A. Z. Hood, and E. Topsakal, "Design of a dual-band implantable antenna and development of skin mimicking gels for continuous glucose monitoring," *IEEE Transactions on Microwave Theory and Techniques*, vol. 56, no. 4, pp. 1001–1008, April 2008.

[25] T. Dissanayake, K. P. Esselle, and M. R. Yuce, "Dielectric loaded impedance matching for wideband implanted antennas," *IEEE Transactions on Microwave Theory and Techniques*, vol. 57, no. 10, pp. 2480–2487, Oct 2009.

[26] W. Liu, S. Chen, and C. Wu, "Bandwidth enhancement and size reduction of an implantable pifa antenna for biotelemetry devices," *Microwave and Optical Technology Letters*, vol. 51, no. 3, pp. 755–757, 2009.

[27] A. Kiourti, M. Tsakalakis, and K. S. Nikita, "Parametric study and design of implantable PIFAs for wireless biotelemetry," in *International Conference on Wireless Mobile Communication and Healthcare*. Springer, 2011, pp. 96–102.

[28] D. H. Werner and Z. H. Jiang, *Electromagnetics of Body-Area Networks: Antennas, Propagation, and RF Systems*. John Wiley & Sons, 2016.

[29] E. Y. Chow, Y. Ouyang, B. Beier, W. J. Chappell, and P. P. Irazoqui, "Evaluation of cardiovascular stents as antennas for implantable wireless applications," *IEEE Transactions on Microwave Theory and Techniques*, vol. 57, no. 10, pp. 2523–2532, Oct 2009.

[30] [Online]. Available: https://www.cst.com/Applications/Article/Evaluation-Of-Implantable-Antennas-In-Anatomical-Body-Models

[31] T. Nagaoka, S. Watanabe, K. Sakurai, E. Kunieda, S. Watanabe, M. Taki, and Y. Yamanaka, "Development of realistic high-resolution whole-body voxel models of japanese adult males and females of average height and weight, and application of models to radio-frequency electromagnetic-field dosimetry," *Physics in medicine and biology*, vol. 49, no. 1, p. 1, 2003.

[32] M. M. Suzan, K. Haneda, C. Icheln, A. Khatun, and K. i. Takizawa, "An ultra-wideband conformal loop antenna for ingestible capsule endoscope system," in *10th European Conference on Antennas and Propagation (EuCAP)*, April 2016, pp. 1–5.

[33] T. Karacolak, R. Cooper, and E. Topsakal, "Electrical properties of rat skin and design of implantable antennas for medical wireless telemetry," *IEEE Transactions on Antennas and Propagation*, vol. 57, no. 9, pp. 2806–2812, Sept 2009.

[34] S. H. Lee and Y. J. Yoon, "Fat arm spiral antenna for wideband capsule endoscope systems," in *IEEE Radio and Wireless Symposium (RWS)*, Jan 2010, pp. 579–582.

[35] S. Yun, K. Kim, and S. Nam, "Outer-wall loop antenna for ultrawideband capsule endoscope system," *IEEE Antennas and Wireless Propagation Letters*, vol. 9, pp. 1135–1138, 2010.

[36] R. Alrawashdeh, Y. Huang, P. Cao, and E. Lim, "A new small conformal antenna for capsule endoscopy," in *7th European Conference on Antennas and Propagation (EuCAP)*, April 2013, pp. 220–223.

[37] P. M. Izdebski, H. Rajagopalan, and Y. Rahmat-Samii, "Conformal ingestible capsule antenna: A novel chandelier meandered design," *IEEE Transactions on Antennas and Propagation*, vol. 57, no. 4, pp. 900–909, April 2009.

[38] B. Lee and F. J. Harackiewicz, "Miniature microstrip antenna with a partially filled high-permittivity substrate," *IEEE Transactions on Antennas and Propagation*, vol. 50, no. 8, pp. 1160–1162, Aug 2002.